Persistent luminescence materials for deep photodynamic therapy

Aurélie Bessière, Jean-Olivier Durand, Camille Noûs

▶ **To cite this version:**

HAL Id: hal-03368806

https://hal.umontpellier.fr/hal-03368806v1

Submitted on 8 Oct 2021

Review

Aurélie Bessière*, Jean-Olivier Durand and Camille Noûs

Persistent luminescence materials for deep photodynamic therapy

Abstract: Persistent luminescence (PerL) materials continue emitting light long after their excitation has stopped. Prepared in the form of nanoparticles they revealed their full potential as bio-nanoprobes for *in vivo* small animal imaging in the last 15 years. PerL materials enable to overcome the limitation of weak light penetration in living tissues. As such, they constitute remarkable light mediators to implement photodynamic therapy (PDT) in deep-seated tissues. This article reviews the recent achievements in PerL-mediated PDT *in vitro* as well as in small animal cancer models *in vivo*. PerL-mediated PDT is realized through the smart choice of a tandem of a PerL material and a photosensitizer (PS). The physical association of the PerL material and the PS as well as their targeting ability is debated. Implants or mesoporous nanoparticles emerge as particularly valuable cargos that further permit multimodality in imaging or therapy. The diversity of charge-trapping mechanisms in a few PerL materials enables a large versatility in the excitation protocols. Although the PerL agent can be pre-excited by UV light before its introduction into the animal, it also induces effective PDT after simple infrared or visible LED illumination across tissues as well as after a mild X-ray irradiation.

Keywords: cancer therapy; nanoparticles; persistent luminescence; photodynamic therapy; photosensitizers.

Persistent luminescence (PerL) occurs in some special luminescent materials that continue emitting their luminescence for minutes or hours after excitation has stopped. This phenomenon, also called long-lasting phosphorescence, long-lasting luminescence or afterglow, has been scientifically described for the first time in 1602 by the alchemist Vincenzo Casciarolo who observed the curious glow of impurity-doped barium sulfide (BaS) present in the now famous Bologna stone. For many decades during the twentieth century copper-doped or (copper, cobalt)-co-doped zinc sulfide (ZnS) formed the commercialized green PerL phosphors used in watch dials, glow-in-the-dark toys and paints. The emergence of rare earths in the 1990s enabled a breakthrough in the field and much more luminous compounds took over. Pioneering green-emitting strontium aluminate $SrAl_2O_4:Eu^{2+},Dy^{3+}$ (SAO:Eu,Dy), revealed in 1996 by Matzusawa et al. [1], was soon followed by blue-emitting $Sr_4Al_{14}O_{25}:Eu^{2+},Dy^{3+}$ [2], $Sr_2MgSi_2O_7:Eu^{2+},Dy^{3+}$ [3] and $Sr_3MgSi_2O_8:Eu^{2+},Dy^{3+}$ (SMSO:Eu,Dy) [4]. These four materials have now become widely available for decoration and emergency displays purposes. The emergence of efficient red-emitting PerL materials is much more recent and their investigation has been promoted by the concept of *in vivo* PerL bioimaging introduced for the first time in 2007 [5]. First generation PerL nanoparticles (PerLNPs) for *in vivo* imaging ($Ca_{0.2}Zn_{0.9}Mg_{0.9}Si_2O_6$: Eu^{2+},Dy^{3+},Mn^{2+} [5] and later $CaMgSi_2O_6:Mn^{2+},Eu^{2+},Pr^{3+}$ [6–9] excited by a simple UV Mercury lamp for a few minutes before their injection to a small animal were able, once injected, to continuously emit a persistent red/near-infrared (NIR) luminescence detectable across the animal tissues for several tens of minutes. This new *in vivo* imaging technique based on a long time-delayed emission relative to the excitation presents two main assets: as the technique totally avoids the excitation of the animal tissues, the observation of deep-seated PerL probes is possible and an excellent signal/noise ratio is obtained due to the complete suppression of autofluorescence. Second generation PerL nanoparticles, made of chromium-doped gallate $ZnGa_2O_4:Cr^{3+}$ (ZGO:Cr) [10] and chromium-doped gallo-germanate $Zn_{1+x}Ga_{2(1-x)}Ge_xO_4:Cr$ (ZGGO:Cr) [11], were soon developed and now constitute the most widely used red-emitting PerL materials for *in vivo* theranostics research in small animals [12, 13]. ZGO:Cr and ZGGO:Cr are not only much brighter than first generation PerL nanoparticles but also able to be re-activated *in vivo* as long as the nanoparticles circulate inside the animal body. This very special

*Corresponding author: Aurélie Bessière, ICGM, Univ. Montpellier, CNRS, ENSCM, Montpellier, France,
E-mail: aurelie.bessiere@umontpellier.fr. https://orcid.org/0000-0003-0082-546X
Jean-Olivier Durand, ICGM, Univ. Montpellier, CNRS, ENSCM, Montpellier, France. https://orcid.org/0000-0003-4606-2576
Camille Noûs, Laboratoire Cogitamus, Paris, France

property widened their field of application, amongst others, to tumor imaging [14]. Since then, PerL nanoparticles have enabled the development of highly versatile imaging experiments. Their charging necessitates a few seconds irradiation, performed either before their injection to the small animal by a UV lamp or after their injection by orange light/808 nm/X-rays, across the animal tissues, at any point of the imaging experiment and as many times as necessary. This versatility enabled interesting achievements in targeting [15–19], drug delivery [20, 21], photothermal therapy [22, 23] and gene therapy [24, 25]. However the most exciting theranostics application of PerL nanoparticles that has emerged in the recent years deals with photodynamic therapy (PDT), which constitutes the topic of this review.

PDT constitutes a high-potential modality [26–30] already recognized for its efficiency and selectivity in the eradication of some types of cancerous or pre-cancerous lesions [31]. The technique relies on the simultaneous presence of light, oxygen and a photosensitizer (PS) at a sub-cellular level. When exposed to light of a specific wavelength, corresponding to its absorption bands, the PS transforms neighboring molecular oxygen or oxygenic species into highly cytotoxic reactive oxygen species (ROS) that cause the tumor necrosis. Most PSs being non-toxic in the dark, PDT action occurs only when and where PS-containing tissues are illuminated, hence guaranteeing a strong selectivity towards the cancerous tissue.

Under light illumination, the PS is excited to a short-lived excited singlet state ($^1PS^\star$) (Figure 1). The excited PS can either decay back to ground state by emitting fluorescence or undergo intersystem crossing whereby the spin of

the electron inverts to form a long-lived triplet state ($^3PS^\star$). In type I reactions, this long-lived state transfers its energy by proton or electron exchange to form radical anions or cations that react with oxygen to produce superoxide anion radicals, hydroxyl radicals or hydrogen peroxides. In type II reactions, the energy of the excited PS is directly transferred to molecular oxygen and leads to $^1O_2$ formation. Both types of products, called ROS, may damage sub-cellular components (plasma membrane, mitochondria, Golgi apparatus, endoplasmic reticulum…) within their lifetime. The latter depends on the PS localization [32]: for $^1O_2$ it was reported to be 0.4 ± 0.2 μs near membranes of living cells [33] and 1.2 ± 0.3 μs *in vivo* in blood vessels [34]. Intracellular diffusion distance is therefore small relative to cell diameter; hence, the effect of ROS generated within a cell is spatially limited to its immediate surroundings. When PDT is applied to cancer, tumor cells or their vasculature are not only irreversibly damaged, but also inflammatory and immune response are triggered and contribute to fighting the tumor growth [35]. PDT is particularly adapted to cancer treatment as PSs tend to accumulate in tumors and light can be conveniently shone to neoplastic tissues when the latter are accessible. Nevertheless PDT is not specific to any type of cell or organelle and also functions against all types of foreign microorganisms (bacteria, fungus and viruses) holding a large potential to cure localized infections [36]. PDT used against pathogenic microorganisms is termed anti-microbial PDT or photodynamic inactivation [37]. Photodynamic inactivation targets microbe external structure without PS penetration into microorganisms hence advantageously avoiding drug resistance
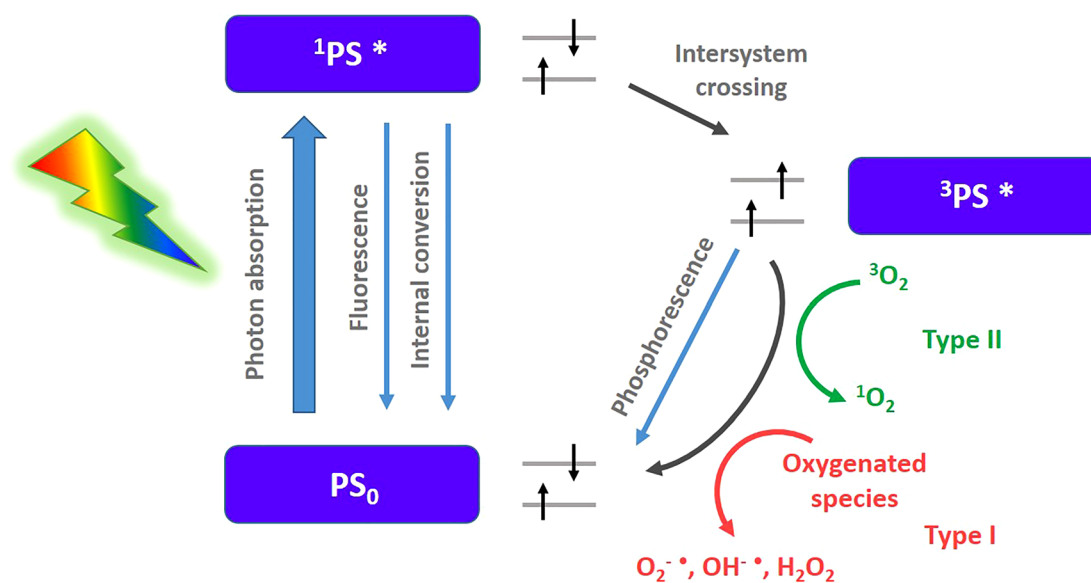
Figure 1: Modified Jablonski diagram showing the role of the photosensitizer (PS) in photodynamic therapy (PDT).

mechanisms [38]. It is therefore highly valuable to fight antibiotic resistance in the case of bacteria like methicillin-resistant *Staphylococcus aureus* [39] or to treat viral infections [40] caused by herpes simplex virus or human papillomavirus [41].

Given the outstanding achievements of PDT for all sorts of localized lesions and in the first place for cancerous tumors, it appears of high interest to tackle its main limitation: the accessibility of the diseased tissue by the excitation light. The visible or NIR light beam used in PDT is strongly attenuated along its penetration path by absorption and scattering processes from the biological components, amongst which water, melanin and hemoglobin [42]. The poor penetration of light in living tissues constitutes the bottleneck of the therapy. Overcoming this limitation would without any doubt revolutionize PDT. It is interesting to note that the same type of limitation, i.e. the short penetration length of light in tissues, has been hindering the otherwise attractive technique of *in vivo* fluorescence imaging [43]. Fluorescence imaging requires a dye excitation, which is impossible across thick biological tissues. Additionally the excitation of the living tissues produces an autofluorescence that hides the probe signal. Given the robust performance of PerL bioprobes for *in vivo* imaging, the latter have naturally appeared as a first choice option for PDT internal light sourcing. This review focuses on the recent achievements of PerL-mediated PDT that constitutes to our opinion a very promising path to overcome the PDT limitation concerning deep-seated targets. The first part of this review highlights the difficulties of current PDT for treating deep lesions at pre-clinical and clinical stages and introduces the options provided by energy transducers. The second part of the review is entirely devoted to PerL materials used as energy transducers for deep PDT.

1 Delivering light to the PSs in deep PDT

When light interacts with matter, i.e. here with living tissue, reflection, refraction, scattering and absorption take place and lead to beam attenuation. Most tissues will scatter light and highly pigmented areas will absorb it due to water, oxyhemoglobin, deoxyhemoglobin, melanin, and cytochromes. The optical penetration depth (i.e. the distance at which the light intensity reduces to 0.37 of the initial intensity), δ, is strongly wavelength-dependent: $\delta < 0.5$ mm at 400–430 nm, 1 mm at 500 nm, 2–3 mm at 630 nm, and 5–6 mm at 700–800 nm (Figure 2) [44]. Hence remarkable achievements were earned with the development of new PSs, whose absorption peaks have been shifted from the UV–visible range towards the infrared. On the clinical end, all possible ways of delivering light internally to the PS have been continuously explored by taking advantage of light-transmitting devices, although often at the cost of more invasiveness. Both these improvements are insufficient to tackle deep-seated lesions or metastasis. Alternative approaches hence consist into introducing molecules, nano-objects or materials that can play the role of internal lights.
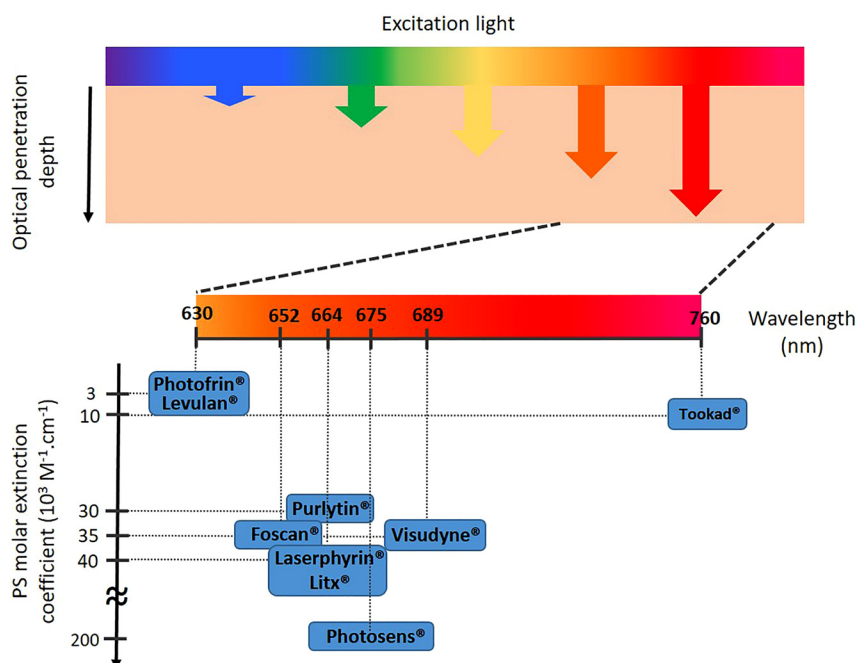
Figure 2: Above: representation of the optical penetration depth of the electromagnetic light spectrum across biological tissues. Below: main clinically approved PSs at their wavelength of therapeutic use.

1.1 Shifting the PS absorption efficiency towards the infrared

Hematoporphyrin (Hp) has been the first identified PS and was directly extracted from the haem co-factor of hemoglobin. In the 1960s, Hp was obtained from water treatment of a blood sample after suppression of iron from the haem molecule. A mixture of Hematoporphyrin derivatives (HpD) was prepared from the action of sulfuric acid, acetic acid and sodium hydroxide on Hp. This mixture always presents a variable composition of Hp oligomers [45, 46]. Commercialized under the brand name Photofrin® in the 1990s, HpD has been the first PS authorized by the US Food and Drug Administration (FDA) for the cancer treatment by PDT (Figure 2). Since then, several other countries also allowed HpD under the brand names Photosan® (Germany), Photogem® (Russia), Haematodrex® (Bulgaria) or Photocarcinorin® (China). The oncologic indications of HpD have been as wide as bladder, esophagus, lung [47], head, neck, abdominal, thoracic, brain, intestinal, skin, breast, and cervical cancer treatment [35, 48, 49]. The injection of HpD to the patient is followed by the illumination of the zone to be treated with red light (630 nm), which penetrates about 3 mm of the living tissue. All porphyrins present a typical absorption spectrum composed of an intense band in the UV-violet (380–500 nm) – the Soret band – where porphyrins present a high molar extinction coefficient ($\varepsilon \approx 4 \times 10^5$ M^{-1} cm^{-1}) and up to four bands of weaker intensity located between 500 and 750 nm – the Q bands – where $\varepsilon \approx 1$–3×10^3 M^{-1} cm^{-1}. Despite the use in oncology of HpD and its high singlet oxygen quantum yield ($\Phi_\Delta = 0.89$ for Photofrin®) this first generation PS presents unfavorable features: (i) HpD accumulates in the skin conferring a severe and long-lasting photosensitivity to the patient (4–6 weeks) (ii) its optical absorption in the red part of the spectrum (Q band) is insufficient ($\varepsilon = 3 \times 10^3$ M^{-1} cm^{-1} at 630 nm for Photofrin®, Figure 2) forcing the injection of a large quantity of HpD (iii) the drug is not pure and its composition hardly reproducible (iv) it presents a poor solubility in polar solvents.

Hence second generation PSs have been developed. In order to avoid skin accumulation and guarantee the formation of pure protoporphyrin IX (PpIX) ($\varepsilon = 5 \times 10^3$ M^{-1} cm^{-1} at 635 nm) [50], a pro-drug based on 5-aminolevulinic acid (ALA), which is the natural precursor for haem formation, was designed. Once ALA is topically applied or injected, a natural retro-control based on the haem bio-synthesis pathway regulates PpIX formation and allows its rapid clearance. ALA application followed by an illumination at 630 nm was US FDA approved in 1999 and commercialized

under the brand name Levulan® for the treatment of actinic keratosis (Figure 2). Further new porphyrinoid PSs have been developed with Q bands shifted to longer wavelength and with larger extinction coefficients (Figure 2) [51]. Several compounds from the chlorin, bacteriochlorin, pheophorbide, bacteriopheophorbide, texaphyrin and phthalocyanine families have emerged [52]. Amongst the chlorin family, meta-tetra(hydroxyphenyl)chlorin (m-THPC) (Foscan®), tin ethyl etiopurpurin (SnET4) (Purlytin®), N-aspartyl chlorin e6 (Ce6) (Laserphyrin®, Litx®) and benzoporphyrin derivative monoacid ring A (BPD-MA) (liposomal formulation, Visudyne®) present a shift of the long wavelength absorption maximum to 652 nm ($\varepsilon = 3.5 \times 10^4$ M^{-1} cm^{-1}, $\Phi_\Delta = 0.87$), 664 nm ($\varepsilon = 3 \times 10^4$ M^{-1} cm^{-1}), 664 nm ($\varepsilon = 4 \times 10^4$ M^{-1} cm^{-1}, $\Phi_\Delta = 0.77$) and 689 nm ($\varepsilon = 3.5 \times 10^4$ M^{-1} cm^{-1}, $\Phi_\Delta = 0.84$), respectively (Figure 2). In the pheophorbide family, 2-(1-hexyloxyethyl)-2 devinyl pyropheophorbide-α (HPPH, Photochlor®) is a highly lipophilic PS that presents an absorption maximum at 665 nm ($\varepsilon = 4.8 \times 10^4$ M^{-1} cm^{-1}, $\Phi_\Delta = 0.48$). It is currently in phase II clinical trials for diverse cancers [53, 54]. In the phthalocyanine family, a quantitative improvement of the extinction coefficient is reached ($\varepsilon = 2 \times 10^5$ M^{-1} cm^{-1}) at a relatively long wavelength (~675 nm). The compounds present a UV–visible absorption spectrum resembling that of porphyrins, i.e. with two main bands. However their Soret band located at around 350 nm is weak whereas their main Q band, located at around 680 nm presents an extremely high intensity with a molar extinction coefficient around 10^5 M^{-1} cm^{-1}, i.e. two orders of magnitude higher than for most porphyrins [55]. Note that their physical and chemical properties can easily be tuned by the introduction of substituents and central metals. Hence Photosens®, an aluminum phthalocyanine (AlPc) actually composed of several sulfonated aluminum chloride phthalocyanines is the only phthalocyanine already approved for clinical use. Currently Photocyanine®, a zinc phthalocyanine (ZnPc), and Pc 4®, a silicon phthalocyanine (SiPc) are under clinical trials [56]. Finally, one of the most promising second generation porphyrinoid PS, branded as Tookad®, is a palladium bacteriopheophorbide that presents a high molar extinction coefficient (10^4 M^{-1} cm^{-1}) at 760 nm. It is currently in the phase of being approved by the FDA for treatment of early-stage localized prostate cancer by interstitial PDT (I-PDT). On the other hand several families of non-porphyrinoid PSs have been investigated although none has received the FDA approval. PSs have been developed from the anthraquinone (hypericin), phenothiazine (methylene blue, toluidine blue), xanthene (rose Bengal (RB), TH9402), cyanine (merocyanine 540) and curcuminoid families. RB (4,5,6,7-tetrachloro-2′,4′,5′,7′-tetraiodo-fluorescein disodium) is a xanthene dye with several chlorine and iodine atoms on

its xanthene rings. It presents an intense absorption band in the green ($\varepsilon = 10^5$ M^{-1} cm^{-1} at 549 nm in water) and a high singlet oxygen quantum yield ($\Phi_\Delta = 0.76$). It is currently an experimental agent for the PDT treatment of breast carcinoma and metastatic melanoma [57].

Alongside the PSs presented here, that are currently or will soon be available in clinics, research is going on for improving the PSs properties to tackle deep-seated tumors. The reader is referred to the excellent review by Fan et al. [58]. Notably two-photon absorption with the use of short-pulsed lasers has been investigated [59] and a certain efficiency has been observed with porphyrins, porphyrazins, tetraphenylporphycenes and difuranonaphthalenes. Two-photon absorption cross-sections have also been significantly improved by incorporating self-assembled porphyrin oligomers into porphyrins [60]. Antenna effects from inorganic nanoparticles such as gold nanorods have also been judiciously exploited [61]. Nevertheless, the overall efficiency remains low with respect to the heating damage caused by a necessarily intense infrared laser irradiation.
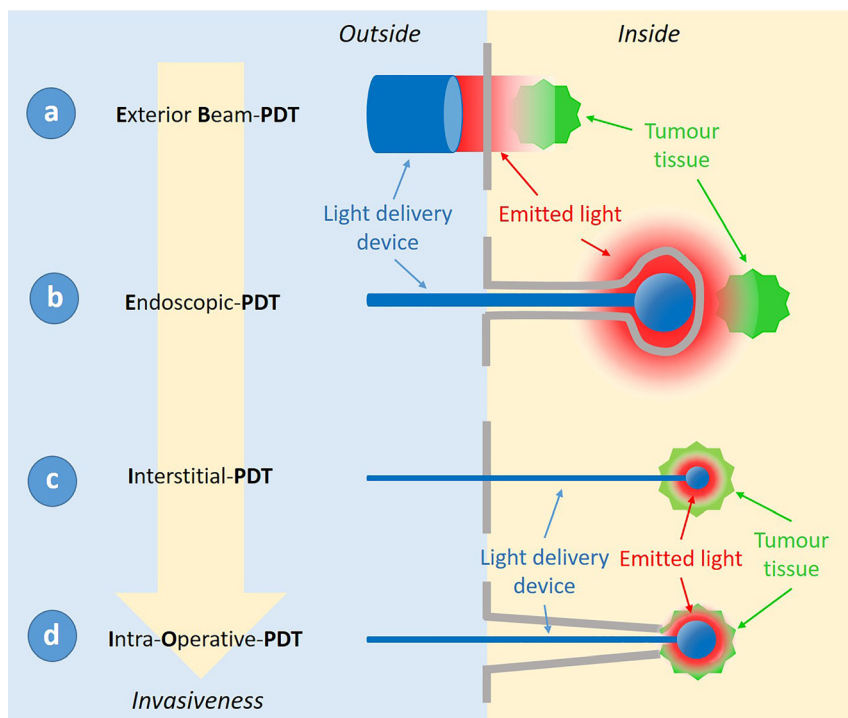
1.2 Light delivery systems in clinical PDT (direct PDT)

The first clinical PDT experiments were carried out in the 1970s by Dougherty et al. who used HpD as PS and a filtered xenon lamp (600–700 nm) directly shone to the patient chest skin to eradicate multiple wall chest cancerous nodules [62]. Since then progress in the PS formulation [50] and in the versatility of light sources [63] allowed many more therapeutic uses and in the first place PDT for skin diseases. After the PS has been orally taken, intravenously injected or topically applied, a lamp, a laser or a LED is shone to the patient diseased skin and Exterior Beam PDT (EB-PDT), also called superficial PDT, is readily realized (Figure 3a). EB-PDT is commonly used for the treatment of oncological or pre-oncological dermatological conditions such as actinic keratosis, Bowen disease and superficial basal cell carcinoma. In the last two decades, EB-PDT has also been used for the treatment of non-neoplastic dermatological ailments such as acne, psoriasis and nail diseases [64]. In the 1990s the development of light diffusers enabled the emergence of Endoscopic PDT (E-PDT) (Figure 3b). Laser or LED light delivered *via* optical fibers introduced into natural canals can reach mucosa that lines the body cavities. A uniform illumination is provided by microlenses, spherical or cylindral diffusors or even diffuser balloons [64]. Hence head and neck [65, 66],

esophagus [67, 68], lung [69] and bladder cancer [70] as well as gynecologic malignant diseases [71] can be successfully treated by E-PDT. For larger tumors, often associated with failure to respond to standard therapy, I-PDT, in which light is delivered intra-tumorally following biopsy canals, is a valuable option [72] (Figure 3c). Optical fibers, often multiple, are inserted into the target tissue *via* needles or placed in catheters implanted percutaneously. The PS in deeply seated tumors or tumors thicker than 10 mm can then be activated. Studies showed positive results in head and neck, prostate, pancreas and brain cancers [72]. Finally, Intra-Operative PDT (IO-PDT) can be carried out as an efficient adjuvant treatment to surgery (Figure 3d). The most striking example concerns malignant gliomas (brain tumors) that usually present a poor prognosis due to the impossibility to resect with an ample safety margin [73, 74]. In 2017, the FDA approved 5-ALA as a fluorescence guidance tool to improve resection of malignant glioma [75, 76]. The injection of 5-ALA was further utilized to realize PDT by illuminating the resection cavity immediately after the surgical act, allowing the killing of adjacent cancerous cells and hence importantly increasing the prognosis [76].

The choice of the light source depends on the target location, PS used, and light dose to be delivered. For the most effective treatment with PDT, the light source must appropriately match the target tissue, delivery device, and PS absorption spectrum. Amongst possible light sources, lamps present the advantage of a simple design, low cost and wide illumination field. However they necessitate the use of filters which results in efficiency loss and are only suited for superficial PDT (EB-PDT) as they cannot be coupled to optical fibers. LEDs present the advantage of being fairly low-cost and portable. LED arrays can be used for endoscopic or interstitial application. However, one of the concerns of using LEDs, especially for I-PDT, is the thermal effect resulting from the low electrical to optical conversion efficiency. Finally, lasers constitute sources of choice for E-PDT or I-PDT. They deliver light with a high optical power, single wavelength emission and a narrow collimated beam that couple well with optical fibers. Lasers also advantageously simplify the dosimetry process.

EB-PDT is ideally straightforward. Acne treatment by EB-PDT already belongs to town medicine. However, the range of applications is limited to skin diseases as energy of incident light falls dramatically at increasing depths below the surface (Figure 1a). E-PDT presents a higher degree of invasiveness. It requires anesthesia, in some cases topical but most often general, and risks of perforation, inflammation or stricture of the endoscopic zone exist. Several placements may be necessary in case of large tumors [67].

Figure 3: Main light delivery systems in clinical PDT for cancerous tumor eradication.

Its efficacy is limited to neoplasms lining the surface of the cavity organ (Figure 3b). In I-PDT invasiveness becomes prominent (Figure 3c). The positioning of the fibers requires a careful treatment planning [77], that necessitates assistance by imaging techniques such as ultrasounds, computed tomography or magnetic resonance imaging [78] and would benefit from real-time dosimetry. Except maybe for the brain, interstitial fibers cannot be left in tissue for a long period. I-O PDT is obviously highly invasive, as it requires open-cranium surgery (Figure 3d) [79]. Deep lesions are therefore treated by PDT at the cost of an increased invasiveness. Their large size or their "bulky" character is always a hindrance to efficient tumor suppression by PDT [44, 63].

1.3 Indirect PDT: mediators for deep PDT

A valuable alternative to direct PDT consists in resorting to PDT mediators able to excite a PS located at depth or inaccessible with direct light illumination. PDT mediators are small objects, with a size ranging from atomic/molecular to nanometer scale, which can easily be delivered to pathological tissues. Amongst them, we will distinguish energy transducers – that convert an external penetrating excitation beam into a radiation of suitable energy to excite the PS - and self-illuminating probes – that do not require any irradiation at all.

1.3.1 Energy transducers

Systems that convert low-energy light (infrared with 750 nm < λ < 1000 nm) or high-energy radiation (X-rays) into visible light are both suitable as energy transducers for PDT. Transducers can convert infrared light by two-photon absorption or up-conversion. Examples of PDT mediated by organic [80] or inorganic two-photon absorption transducers exist but remain scarce, gold nanorods constituting the most representative example of inorganic transducers of that type [81–83].

Lanthanide-doped up-converting nanoparticles (UCNP) used as PDT mediators have been more investigated as they present a higher conversion efficiency [84–93]. Although up-conversion remains a low yield process compared to classical Stokes luminescence, the transducer-PS systems can benefit from an efficient energy transfer if the transducer-PS distance is kept short. In practice, PSs are either loaded into the pores of a shell nanoparticle that embeds an UCNP [89, 94] or covalently bound to an UCNP [87]. Although the latter is more challenging in terms of preparation, it guarantees an optimum energy transfer [95]. Two important limitations neverthe-less exist when an infrared external excitation is used. First, infrared light penetration, although longer than visible light, does not exceed 1.5 cm for up-conversion luminescence imaging and *a fortiori* for PDT mediation [96]. Secondly laser heating cannot be neglected in the

infrared range, which constitutes a severe side-effect of the technique particularly at 980 nm where water strongly absorbs NIR light [97].

On the other hand the use of X-rays to activate PS has recently triggered a large interest. In the last three years not less than 10 review papers have dealt with nanosystems activated by X-rays to treat cancerous tumors [98–107], five of them being specifically dedicated to X-ray activated PDT (X-PDT) [99, 101, 102, 104, 106]. Indeed X-rays present a virtually unlimited penetration ability in living animals. In diagnosis imaging (computed tomography) 30–70 keV energy X-rays are used while in radiotherapy photon beam energies range from superficial (30–80 keV), through orthovoltage (100–300 keV), to megavoltage energies (5–25 MeV) [108]. Megavoltage energies are used to treat deep seated tumors [109]. Since around 60% of all cancer patients receive a radiotherapy treatment and X-ray computed tomography has become a major medical imaging tool [110], X-ray beam equipment is readily available in clinics. The challenge in X-PDT resides in lowering, if possible drastically, the dose delivered to the patient as compared to radiotherapy standard by using nanoscintillators, i.e. down-converting nanomaterials yielding radioluminescence under X-rays. Their radioluminescence serves to activate the PS and trigger PDT. The concept was first reported by Chen et al. in 2006 [111]. Since then, several types of nanoscintillators have been tested in solutions, from nanoparticles made of traditional scintillating crystals constituted of heavy atoms to metals, metal-organic frameworks and quantum dots. The challenging stage of *in vitro* X-PDT has been successfully reached in a few examples: Y_2O_3 nanoparticles coupled to psoralen on PC-3 human prostate cancer cells [112], LaF_3:Tb nanoparticles coupled to *meso*-tetra(4-carboxyphenyl)porphyrin on brain cancer cells [113], CeF_3:Tb,Gd nanoparticles coupled to RB on 4T1, Renca and Mgc803 cells [114], Y_2O_3 nanoparticles alone [115] and ultra-small nanoparticles chelated with terbium coupled to 5-(4-carboxyphenyl succinimide ester)-10,15,20-triphenyl porphyrin [116]. Only a few teams further achieved *in vivo* PDT in mice with SAO:Eu^{2+} nanoparticles coupled to merocyanine 540 [117], $LiYF_4$ nanoparticles coupled to ZnO [118], $NaGdF_4$:Tb nanoparticles coupled to RB [119], $Gd_2(WO_4)_3$:Tb nanoparticles coupled to merocyanine 540 [120], Zn_2SiO_4:Mn nanoparticles coupled to RB [121], $NaLuF_4$:Tb nanoparticles coupled to RB [122] and CaF_2:Ce,Tb nanoparticles coupled to RB [123]. Note that all these results should be taken with care as they were not conducted on orthotopic models. Interestingly some of these materials presented as scintillators (SAO:Eu^{2+} and NaXF$_4$:Tb^{3+} with X = Gd,Lu) may also present persistent luminescence as PerL has been reported for

SAO:Eu^{2+} [124], $NaLuF_4$:Pr^{3+} [125], $NaYF_4$:Tb^{3+} (NYF:Tb^{3+}) [126] and Na(Gd,Lu)F_4:Tb^{3+} [127], which may explain why the dose used to perform X-PDT is lower in these examples.

1.3.2 Self-illuminating probes

Self-illuminating systems are based on chemiluminescence, bioluminescence or Cerenkov radiation. They constitute interesting candidates as internal light sources for PDT [128, 129].

Chemiluminescence is a process by which light is generated through chemiexcitation during a chemical reaction [130]. The most famous systems are luminol–H_2O_2 and oxalate ester–H_2O_2 [131]. Molecules such as luminol and derivatives [132] or enzymes such as luciferase are able to generate intrinsic light, which then activates PSs through chemiluminescence resonance energy transfer (CRET) or bioluminescence resonance energy transfer (BRET), respectively. The field has been comprehensively reviewed [133]. BRET technique allowed to excite different kinds of PSs, such as Photofrin®, tetraphenyl porphyrin, RB, Ce6, Foscan® *via* FRET from quantum dots, carbon dots conjugated to PpIX, oligomeric *p*-phenylene vinylene (OPV). More recently, ROS generating proteins have been fused with luciferase for the targeting of breast cancer through BRET [134]. Furthermore, a recent paper showed that PEI-modified calcium phosphate nanoparticles loaded with hypericin, D-luciferin and pDNA coding for luciferase enzyme were efficient in inducing tumor regression in mice after intra-tumoral (IT) injection of the functionalized nanoparticles [135]. BRET process thus represents a promising cancer modality treatment.

Cenrenkov radiation is a continuous spectrum from UV-near IR energies (the number of photons for each wavelength following a 1/lambda function) resulting from the interaction between a charged particle and a dielectric medium provided that the particle speed is higher than velocity of light [136]. Such particles typically arise from radionuclides with β-emissions such as ^{18}F, ^{64}Cu, ^{68}Ga… etc. A few authors hence carried out PDT in small animal models *via* Cerenkov Radiation Energy Transfer (CeRET) from radionuclides to PSs. In first realizations radionuclides and PSs (deoxy-2-[^{18}F]fluoro-D-glucose and apotransferrin and titanocene-charged TiO_2 nanoparticles as the first instance [137]) were co-injected. In later examples radionuclides and PSs were co-localized within a nano-agent (^{89}Zr and Ce6 loaded in hollow mesoporous silica as the first example [138]).

When PDT is mediated by self-illuminating probes, one may lose the specificity that is provided by external light illumination in direct PDT. This is particularly true for

CeRET-assisted PDT systems that function regardless of their microenvironment. On the contrary, in CRET and BRET-assisted PDT, a certain specificity is reestablished as the oxidative IT environment often favors the chemiluminescence reactions.

2 Persistent luminescence mediators for PDT

In Section 1.3 we have classified the mediators to achieve PerL-mediated PDT into "a. Energy transducers" and "b. Self-illuminating probes". PerL materials would situate half-way between the two categories. They can indeed theoretically be used as self-illuminating probes, when they are charged (excited) outside the animal body prior to their injection, similarly to the way they have first been used in small animal imaging [5, 8]. However most often one would favor an additional *in situ* excitation for practical reasons. One may desire to temporally control the triggering of light emission and the beginning of the PDT process. Besides efficiency is enhanced when PerL emission occurs not long after charging. In that case, PerL materials fall into the category of energy transducers.

Note that PerL materials appear particularly suited for PDT for the following reason. Unlike radiotherapy where light radiation doses have a deleterious effects because they encourage cell repair and radiation resistance, light provided at low-intensity fluence over long periods has proved more beneficial for PDT efficiency than intense light delivered over a short period. This phenomenon has been termed as metronomic PDT, in reference to metronomic chemotherapy in which several small doses of drug are advantageously administered instead of a unique heavy dose [139, 140]. In PDT this phenomenon is explained by the temporary oxygen deficit that results from the oxygen-consuming PDT process itself. Hence, a low-intensity illumination enables the system to constantly retrieve its oxygen supply. Since persistent luminescence is by essence a long and low-intensity light, it appears as particularly suited for a metronomic PDT action.

2.1 Choice of the PerL material/PS couples in PerL-mediated PDT

To ensure optimum efficiency one should aim at a significant spectral overlap between the emission spectrum of the PerL material and the PS absorption spectrum. Amongst the reported examples of PerL-mediated PDT, we find a few examples of blue/green-emitting afterglow materials whereas the vast majority deals with red-emitting PerL materials.

In the category of blue/green-emitting PerL materials, Homayoni et al. [141] reported PDT with $Sr_3Al_2O_8$:Eu^{2+},Dy^{3+} as the PerL material. The emission spectrum of the latter consists of a broad band due to Eu^{2+} $5d$–$4f$ transition peaking at 460 nm and extending over 430–520 nm [142]. $Sr_3Al_2O_8$:Eu^{2+},Dy^{3+} nanoparticles were coupled to the PS PpIX, which presents an intense and broad Soret band peaking at 405 nm and rapidly dropping to zero around 450 nm [143]. Hence the PerL spectrum is superimposed only to the long-wavelength tail of the Soret band of PpIX but the system benefits from the particularly high extinction coefficient of PpIX at 405 nm ($1,24 \times 10^5$ M^{-1} cm^{-1}). A second example of green-emitting PerL material tested for PDT is the well-known SAO:Eu,Dy. The choice was guided by the bright luminosity of SAO:Eu,Dy that emits a broad band spectrum due to Eu^{2+} $5d$–$4f$ transition, peaking at 520 nm (450–600 nm) [1], which led the authors to select RB as the PS [144]. RB absorption spectrum is double-peaked with maximum intensity at 560 nm (475–580 nm) (Figure 4a), so that we can estimate that less than a third of SAO:Eu,Dy PerL is optimally harvested. Finally Ma et al. [145] associated ZnS:Cu,Co PerL nanoparticles presenting a broad green band peaking at 546 nm (460–680 nm) with the PS tetrabromorhodamine-123 (TBrRh123) that shows an absorption band peaking at 518 nm (450–550 nm). Again, we can evaluate from Figure 4b that only around a third of the PerL light is optimally harvested. Most recently Hu et al. reported NYF:Tb^{3+} nanoparticles associated with the photocatalyst g-C_3N_4 [126]. They revealed in NYF:Tb^{3+} a super-long green persistent luminescence (>240 h) obtained after X-ray charging. NYF:Tb^{3+} PerL proceeds *via* Tb^{3+} f–f transitions, i.e. emits a high-intensity line at 543 nm ($^5D_4 \rightarrow {}^7F_5$) and six medium-intensity lines at 380 nm ($^5D_3 \rightarrow {}^7F_6$), 410 nm ($^5D_3 \rightarrow {}^7F_5$), 435 nm ($^5D_3 \rightarrow {}^7F_4$), 485 nm ($^5D_4 \rightarrow {}^7F_6$), 580 nm ($^5D_4 \rightarrow {}^7F_4$) and 620 nm ($^5D_4 \rightarrow {}^7F_3$). Hence g-$C_3N_4$ that only absorbs over the 350–430 nm range [126] harvests only about a third of Tb^{3+} PerL emission.

Red-emitting ZGO:Cr and ZGGO:Cr PerL materials represent two thirds of the PerL-mediated PDT experiments conducted *in vitro* (Table 1) and three quarters of the ones conducted *in vivo* (Table 2). ZGO:Cr and ZGGO:Cr proved themselves potent as *in vivo* imaging probes for tumor targeting [17, 18], gastro-intestinal tract trafficking [153], probiotics tracing [154], glycan targeting [15], cancer
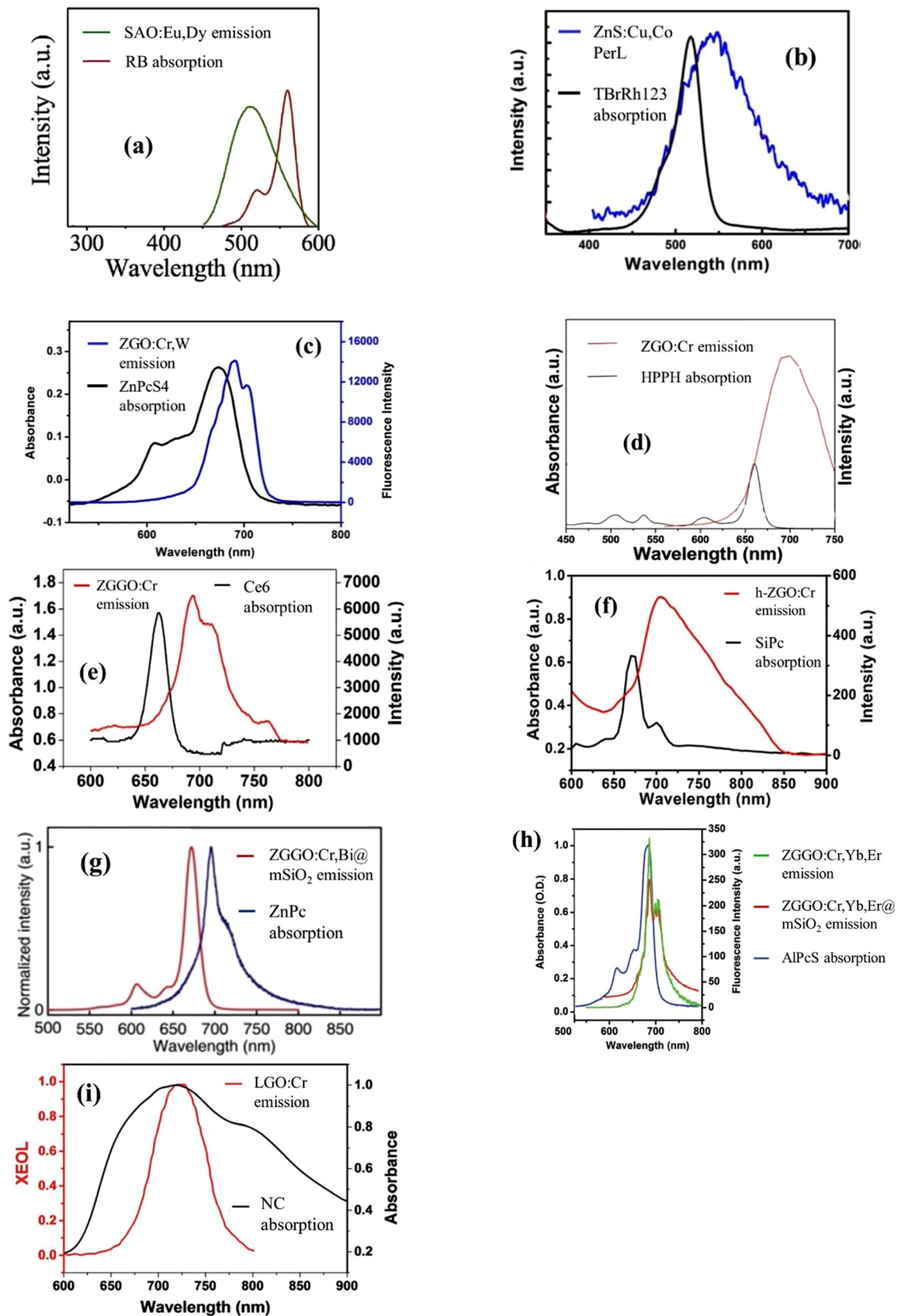
Figure 4: PerL materials emission spectra in correspondence to PSs absorption spectra in several examples of PerL-mediated PDT. The PerL material/PS couples are: (a) SAO:Eu,Dy/RB [144] (b) ZnS:Cu,Co/TBrRh123 [145] (c) ZGO:Cr,W/ZnPcS4 [146] (d) ZGO:Cr/HPPH [147] (e) ZGGO:Cr/Ce6 [148] (f) h-ZGO:Cr/SiPc [149] (g) ZGGO:Cr,Bi@mSiO$_2$/ZnPc [150] (h) ZGGO:Cr,Yb,Er/AlPcS [151] (i) LGO:Cr/NC [152]. Reproduced with permissions from [144–152].

metastasis targeting [155], and stem cell tracking [19], PerL imaging has also been conveniently coupled to a second imaging modality like X-ray computed tomography [156], magnetic resonance imaging [157–161] and nano-thermometry [162] (multi-modality). Furthermore ZGO:Cr and ZGGO:Cr have been associated with therapeutic agents for chemotherapy [20], photothermal therapy [23], gene therapy [25] and of course PDT as related in this review (theranostics). To decline such a variety of uses, their shape (size of nanoparticles [17, 163, 164] embedment into porous nanoparticles [165, 166] or into implants [148]) and chemical composition (co-doping) [16, 19, 158, 166–170] have been adjusted with versatility. ZGO:Cr and ZGGO:Cr emission spectra consist in several zero phonon lines due to $^2E\ (^2G) \rightarrow\ ^4A_2\ (^4F)$ transition of several types of Cr^{3+} ions present in slightly different environments accompanied by their phonon lines [171]. At room temperature, ZGO:Cr and ZGGO:Cr PerL spectra peak at 695 nm, extending over 650–750 nm for ZGO:Cr [10] and over 680–850 nm for ZGGO:Cr [11]. Accordingly, these materials have been associated with last generation PSs whose emission is shifted towards the NIR and that mainly belong to pheophorbides, phtalocyanines and chlorins. In examples of Table 1 and Table 2, ZGO:Cr has been associated to HPPH [147], Zn(II) phtalocyanine tetrasulfonic acid (ZnPcS4) [146], SiPc [149] and IR780 (2-[2-[2-Chloro-3-[(1,3-dihydro-3,3-dimethyl-1-propyl-2H-indol-2-ylidene) ethylidene]-1-cyclohexen-1-yl]ethenyl]-3,3-dimethyl-1-propylindolium iodide) [172] while ZGGC has been coupled to SiPc [155, 173, 174]), AlPcS [151], ZnPc [150] and Ce6 [148]. The spectral match between ZGO:Cr and ZnPcS4 (Figure 4c) or IR780 [172] is quite satisfying whereas HPPH appears largely blue-shifted relative to ZGO:Cr and optimally harvests only one tenth of the PerL emission (Figure 4d). When the PerL material shifts its emission towards the infrared with hollow ZGO:Cr or with ZGGO:Cr, it is even more difficult to obtain well corresponding spectra. Ce6 (Figure 4e) [148], SiPc (Figure 4f) [149], ZnPc (Figure 4g) [150], and AlPcS (Figure 4h) [151] all appear blue-shifted relative to the PerL emission. Finally the example of $LiGa_5O_8{:}Cr^{3+}$ (LGO:Cr) coupled to 2,3-naphtalocyanine (NC) [152] presents the most appropriate spectral match as NC absorption spectrum is broader than LGO:Cr PerL emission spectrum (Figure 4i).

Overall, the spectral match is not ideal in the reported examples as the PSs absorption spectra often lack a sufficiently broad spectral width as compared to the PerL emission spectra. As a consequence the efficiency of PerL-mediated systems could certainly be improved by the use of PSs with broader spectral width or conversely the use of PerL materials with narrower spectral width.

2.2 Charging the PerL material

2.2.1 Trapping and de-trapping mechanisms in PerL materials

Although the scientific community agrees on the description of persistent luminescence as resulting from trapped charge carriers at point defects of a crystalline material followed by their progressive thermal detrapping that continuously feeds the optical centers, the identification of point defects at stake and the exact mechanism of charge trapping and detrapping are on-going objects of debate in many PerL materials [176–180]. Furthermore mechanisms have been mostly investigated in bulk crystalline materials (crystals or micro-crystalline powders) following the tradition of crystal optics. With the application of bioprobe, interest has shifted towards nanoparticles, where persistent luminescence can still be observed but for which mechanisms are modified compared to their bulk counterpart. Surface effects complicate the description of the phenomenon.

With first generation PerL bioprobes conceived for small animal imaging, the PerL materials were meant to be charged (excited) with UV light *before* they enter the biological medium (cell or animal) so that UV light does not cause any damage to and does not need to pass through the living tissues. The choice of UV light is advantageous in terms of cost as a simple Mercury lamp is sufficient to excite the long-lasting phosphorescence of a PerL bioprobe. Furthermore, UV light has been the traditional way to excite PerL materials that typically present a bandgap energy of 4–10 eV. In Figure 5, (I)(1), (I)(2) and (I)(3) illustrate the type of mechanisms at stake when UV light is used to charge a PerL material. An excitation of energy higher than bandgap creates holes in the valence band (VB) and electrons in the conduction band (CB) ((I)(1) in Figure 5). Free carriers can then be trapped at point defects of the material. In (I)(1) the hole is captured by the luminescent center A while the electron is trapped at a defect B. Alternatively with UV or in some cases with visible (mostly blue) excitation, PerL materials can also be excited *via* the charge transfer band of a dopant, as schematized in the scheme (I)(2) of Figure 5. This is typically the case of materials doped with Cu^+ and Mn^{2+} like $ZnS{:}Cu^+$ or $MgGeO_3{:}Mn^{2+}$ [177]. A third classical mechanism involves the efficient *f–d* transitions of bi- or tri-valent lanthanide ions such as

Table 1: Experimental results of *in vitro* PerL-mediated PDT realized in living cells. *PCM = Phase Change Material (here oleic acid + hexadecanol). **Assessed by MTT assay unless precised otherwise. ***Assessed by a cell counting kit (CCK-8) using WST-8 (2-(2-methoxy-4-nitrophenyl)-3-(4-nitrophenyl)-5-(2,4-disulfophenyl)-2H-tetrazolium, monosodium salt). ****Assessed by Trypan Blue viability test. *****Assessed by BacLight Live/Dead Bacterial Viability Kit (L-7012;Molecular Probes).

References	PerL host material family	PerL source	Shape	PS	Surface	Type of cells	Excitation protocol	Cells viability**
[144]	SAO	$SrAl_2O_4$:2%Eu^{2+},4%Dy^{3+} + $NaYF_4$:25%Yb^{3+},0.5%Tm^{3+} (up-converter)	Implant (PDMS-PerL-PS)	RB	–	HT29 (human colon cancer)	5s 980 nm laser (2 W/cm²) = 1 cycle	73% after one cycle***, 60% after two cycles***, 48% after three cycles***, 36% after four cycles***
[145]	ZnS	ZnS:Cu,Co	PerLNP-PS conjugate	TBrRh123	–	PC3 (human prostate cancer)	1 min X (2 Gy)	40%
[152]	LGO	$LiGa_5O_8$:Cr	PerLNP@m-SiO_2@PS	NC	–	H1299 (human non-small cell lung cancer)	X (2 Gy)	46.4%, 50.2% (through 1.6 cm thick tissue), 60.1% (through 2.8 cm thick tissue)
[141]	SMSO	$Sr_3MgSi_2O_8$:Eu^{2+},Dy^{3+}	PerLNP-PS conjugate	PpIX	FA	PC3 (human prostate cancer)	5 min UV	~15%/PpIX alone
[175]	ZGO	$ZnGa_{1.995}O_4$:0.005Cr^{3+}	PerLNP	–	OH	MDA-MB-231 (human breast cancer) MCF-7 (human breast cancer)	5 min UV pre-irradiation	24%/9% without UV irradiation****, 34%/8% without UV irradiation****
[147]		$ZnGa_{1.996}O_4$:$Cr_{0.004}$	Separate PerLNP and PS	HPPH	–	U87MG (human glioblastoma)	2 min white LED = 1 cycle	82% after one cycle, 23% after three cycles
[146]		$ZnGa_{1.99}O_4$:0.005Cr^{3+},0.005W^{6+}	PerLNP-PS conjugate	ZnPcS4	–	S180 (murine sarcoma) HeLa (human cervical cancer)	2 min X (0.18 Gy), three cycles (every 40 min)	19%***, 23%***
[172]		$ZnGa_2O_4$:0.004Cr^{3+}	PCM* nanoparticle encapsulating PS and PerLNP	IR780	–	HeLa (human cervical cancer)	5 min 808 nm laser (0.4 W cm⁻²) for PCM* melting + 5 min white LED (1000 lm)	18%
[173]	ZGGO	$Zn_3Ga_4Ge_2O_{13}$:0.3%Cr^{3+}	PerLNP-PS conjugate	SiPc	–	HepG2 (human liver cancer)	10 min 254 nm UV pre-irradiation + 808 nm laser (1 W cm⁻²)	50% 3 min laser irradiation

Table 1: (continued)

References	PerL host material family	PerL source	PS	Shape	Surface	Type of cells	Excitation protocol	Cells viability**
								23% 5 min laser irradiation 5% 10 min laser irradiation
[151]		$Zn_{1.25}Ga_{1.5}Ge_{0.25}O_4{:}0.5\%Cr^{3+},2.5\%Yb^{3+},0.25\%Er^{3+}$	AlPcS	PerLNP@m-SiO$_2$@PS	–	HeLa (human cervical cancer)	Fractionated 405 nm (8 J cm^{-2})	8%/87% with AlPcS alone 1% three days later
[155]		$Zn_{1.25}Ga_{1.5}Ge_{0.25}O_4{:}0.5\%Cr^{3+},2.5\%Yb^{3+},0.25\%Er^{3+}$	SiPc	PerLNP-PS@h-SiO$_2$@DOX	CCM	4T1 (murine breast cancer)	200 s 808 nm laser	2% (with DOX release)
[148]		$Zn_{1.25}Ga_{1.5}Ge_{0.25}O_4{:}0.5\%Cr^{3+},2.5\%Yb^{3+},0.25\%Er^{3+}$	Ce6	Implant (alginate Ca^{2+} hydrogel)	–	4T1 (murine breast cancer)	5 min UV + 3 min red light (0.7 W cm^{-2})	60% 18%
[174]		$Zn_3Ga_2GeO_8{:}Cr^{3+},Yb^{3+},Er^{3+}$	SiPc	PerLNP@m-SiO$_2$@PS	PEG	HepG2 (human liver cancer)	X (4 Gy)	53%
[150]		$Zn_2Ga_{2.98}Ge_{0.75}O_8{:}0.02Cr^{3+},0.12Bi^{3+}$	ZnPc	PerLNP@mSiO$_2$-PS	–	Hepa1-6 (murine hepatoma)	10 min 635 nm laser (150 mW cm^{-2}) pre-irradiation	18%
[126]	NYF	$\beta\text{-}NaYF_4{:}10\%Tb^{3+}$	g-C$_3$N$_4$	Separate PerLNP and PS	–	Bacteria *Pseudomonas aeruginosa* (PAO1)	2 min (30 mA, 40 kV) X	67.14%, 30.92% 5 h later*****

Table 2: Experimental results of *in vivo* PerL-mediated PDT realized in small animal cancer models. *PCM = Phase Change Material (here oleic acid + hexadecanol). **LP = Liposome. ***DSPE-PEG = 1,2-Distearoyl-Sn-glycero-3-PhosphoEthanolamine-*N*-methoxy(PolyEthylene Glycol).

References	PerL host material family	Cancer small animal model	PerL source	PS	Shape	Surface	Excitation protocol	Result
[144]	SAO	100 mm³-large subcutaneous tumor induced by injection of HT29 cells in the arm	$SrAl_2O_4$:2%Eu^{2+},4%Dy^{3+} + $NaYF_4$:25%Yb^{3+},0.5%Tm^{3+} up-converter	RB	Implantation of PDMS-PerL-PS implant onto the tumor surface	–	5 s 980 nm laser (2 W/cm²) twice a day	Tumor size = 50% that of control after 15 days, tumor completely suppressed by addition of O_2 producing agent in the implant
[152]	LGO	Tumor induced by percutaneous injection of H1299 cells into lateral thorax	$LiGa_5O_8$:Cr	NC	IV injection of PerLNP@m-SiO_2@PS	PEG + cetuximab	X (6 Gy)	Tumor size = 8% that of control after seven days
[147]	ZGO	6–8 mm-diameter tumor induced by subcutaneous injection of U87MG cells	$ZnGa_{1.996}O_4$:$Cr_{0.004}$	HPPH	IT injection of PLGA/NMP-PerL implant	–	IV injection of HPPH at day 1 and at day 8.15 min white LED after each injection.	Tumor size = 8% that of control after 15 days
[146]		6–8 mm-diameter tumor induced by injection of S180 cells	$ZnGa_{1.99}O_4$:0.005Cr^{3+},0.005W^{6+}	ZnPcS4	IV injection of PerLNP--PS conjugates	–	IV injection at day 0 and at day 7.2 min X (0.18 Gy) 4h after each injection.	Tumor size = 10% that of control after 16 days
[172]		80 mm³-large tumor induced by subcutaneous injection of HeLa cells	$ZnGa_2O_4$:0.004Cr^{3+}	IR780	IV injection of PCM*-PS-PerL NP	Lecithin/DSPE-PEG***	IV injection every two days. 5 min 808 nm laser (0.4 W cm⁻²) for PCM* melting + 5 min white LED (1000 lm), 12 h after each injection.	Total ablation after 4–6 days without any recrudescence
[149]		80 mm³-large tumor induced by subcutaneous injection of 4T1 cells in the flank	$ZnGa_2O_4$:0.001Cr^{3+}	SiPc	IT injection of h-PerLNP@PS	–	IT injection at day 1 and at day 7.10 min white LED after each injection	Tumor size = 5% that of control after 14 days
[173]	ZGGO	60–80 mm³-large tumor induced by subcutaneous injection of HepG2 cells	$Zn_3Ga_4Ge_2O_{13}$:0.3%Cr^{3+}	SiPc	IT injection of PerLNP--PS conjugates	–	10 min 254 nm UV pre-irradiation for 10 min + 808 nm laser (1 W cm⁻²) 4 h after injection	Total ablation after 16 days

Table 2: (continued)

References	PerL host material family	Cancer small animal model	PerL source	PS	Shape	Surface	Excitation protocol	Result
[155]		Mammary tumor (with metastasis) induced by subcutaneous injection of 4T1 cells in the breast	$Zn_{1.25}Ga_{1.5}Ge_{0.25}O_4$:0.5%$Cr^{3+}$,2.5%$Yb^{3+}$,0.25%$Er^{3+}$	SiPc	IV injection of h-SiO_2@PerLNP-PS, DOX	CCM or LP**	20 min UV pre-irradiation before injection + 200 s 808 nm laser (3 W cm^{-2}) 4 h after injection	99% inhibition relative to control after 21 days
[148]		0.5–0.8 cm^3-large tumor induced by subcutaneous injection of 4T1 cells in the back	$Zn_{1.25}Ga_{1.5}Ge_{0.25}O_4$:0.5%$Cr^{3+}$,2.5%$Yb^{3+}$,0.25%$Er^{3+}$	Ce6	IT injection of alginate Ca^{2+} hydrogel-PerLNP implant	–	IT injection of 5 min 254 nm UV pre-irradiated implant 2 h after Ce6 IV injection. 10 min red light (1 W cm^{-2}) 3 h after Ce6 IV injection	Tumor size = 6% that of control after 15 days
[174]		Tumor induced by injection of HepG2 cells	$Zn_3Ga_2GeO_8$:Cr^{3+},Yb^{3+},Er^{3+}	SiPc	IV injection of PerLNP@m-SiO_2@PS	PEG	IV injection of m-PerLNP@PS at day 1 and at day 4 4.4 Gy × 8 h after each injection	Tumor bioluminescence signal = 6% that of control after 16 days
[150]		Tumor induced by injection of Hepa1-6 cells	$Zn_2Ga_{2.98}Ge_{0.75}O_8$:0.02$Cr^{3+}$,0.12$Bi^{3+}$	ZnPc	IV injection of PerLNP@mSiO$_2$-PS	–	10 min 635 nm laser (150 mW cm^{-2}) 3h after injection	Tumor size = 2% that of control after 14 days

Eu^{2+}, Ce^{3+}, Tb^{3+} and Pr^{3+} introduced as dopants. These absorption transitions can lead to the optical center auto-ionization when the dopant excited state is situated inside or close to the bottom of the host CB (mechanism (I)(3) in Figure 5). This is the type of mechanism that Clabau et al. [178] as well as Dorenbos et al. [181] proposed to explain the afterglow of SAO:Eu,Dy. Similarly to mechanism (I)(1), mechanisms (I)(2) and (I)(3) also permit the delocalization of electrons that can freely move in the material until they get trapped at point defects. Most of the PerL materials used for green- or blue-emitting displays, being charged by natural UV/blue light during the day and re-emitting at night, function according to these mechanisms. In first generation *in vivo* imaging PerL materials, the same type of mechanism takes place. Lecointre et al. [182] and Maldiney et al. [8] showed that $Ca_{0.2}Zn_{0.9}Mg_{0.9}Si_2O_6:Mn^{2+},Eu^{2+},Dy^{3+}$ and $CaMgSi_2O_6:Mn^{2+},Eu^{2+},Pr^{3+}$, respectively, were effectively charged through the $f-d$ transition of Eu^{2+} at 254 nm or 350 nm as represented by the mechanism (I)(3) in Figure 5 while their band-gap energy is at much higher energy (8.4 eV/147 nm). A few years later ZGO:Cr demonstrated a two orders of magnitude improvement in PerL

Figure 5: Types of mechanisms at stake in PerL materials used in PerL-mediated PDT. For sake of simplicity, in the mechanisms displayed here, the hole is captured by the optical center A while the electron is trapped at the defect center B or C. The reverse mechanism can be drawn with an electron at the optical center and a hole at the defect center.

intensity relative to the previous silicates. At that time, ZGO:Cr was also charged by UV light by exciting ZGO:Cr across its bandgap (4.4 eV) according to a mechanism of type (I)(1) (Figure 5) [10]. Optimum charging by mechanism (I)(1), (I)(2) or (I)(3) takes between a few seconds and a few minutes after which period the excitation can be switched off. PerL emission then results from a thermally activated process represented by mechanism (a) in Figure 5 and characterized by the electron trap depth E_T. PerL decay is governed by the lifetime of the trapped electron expressed by an $\exp(E_T/k_B T)$ law. Hence, the PerL imaging technique still presented an important restriction inherent to the limited decay period of the PerL materials and the imaging time was typically limited to a couple of hours after the injection of the PerLNPs. Since nanoparticles accumulation in tumors by Enhanced Permeation and Retention (EPR) effect often takes more than 4 h, by which the PerL signal had drastically fainted, tumor imaging was hardly possible. Hence a new generation of PerL bioprobes was developed.

Second generation PerL bioprobes possess the quality of being excitable or re-excitable *in situ*, whether *in vitro* for cell imaging or *in vivo* for animal models. Therefore, the bioprobe persistent luminescence can conveniently be triggered at any time after the incubation or the injection into the biological medium. Note that the excitation period remains short, typically a few minutes, whereas the subsequent imaging phase lasts for a few tens of minutes or a few hours. The *in situ* excitation constitutes either a primary charging process of the bioprobe or an additional charging excitation in order to enhance the PerL signal when the bioprobe had primarily been excited *ex vivo*. In both cases, the excitation needs to be harmless to the biological medium and able to penetrate the living tissues as deeply as possible. The absolute satisfaction of both these conditions is impossible and in practical, one can distinguish three types of realizations.

In a first type of systems, X-ray is the excitation source as it is able to go through living tissues over a virtually unlimited depth. The PerL material should ideally be an X-ray excitable scintillating material presenting afterglow. In the field of scintillators, afterglow is defined as long-lasting phosphorescence occurring after the charging phase during which the scintillator is exposed to radiation. Its mechanism of charging can also be represented by mechanism (I)(1) in Figure 5 but X-rays enable the production of a huge amount a free electrons–holes pairs. For bioimaging application, X-ray excitation presents the advantage of reaching zones located at depth in living tissues although the dose should then be carefully watched.

In a second type of systems, red light is the excitation source as it shows an acceptable penetration depth, at least in small animal models. The PerL material must have the specific property of being excitable in the red range, which excludes most of the long-lasting phosphors known to date. In practical, it means that during the excitation phase, charges (holes and/or electrons) are trapped through a localized mechanism around the luminescent ion as represented by mechanism (II) in Figure 5, since the excitation energy is less than band gap or charge transfer energy. The charging process is relatively less powerful than through mechanisms (I)(1), (I)(2) and (I)(3) but it was proved efficient enough for *in vivo* applications [14]. Mechanisms have been investigated in detail in ZGO:Cr and described in a multiplicity of ways to comprehend the phenomenon thoroughly (Figure 6) [171, 183]. In ZGO:Cr, holes and electrons are not separated between the luminescent center and a neighboring defect. Instead, when Cr^{3+} is excited from its $^4A_2(^4F)$ fundamental level to its $^4T_2(^4F)$ or $^4T_1(^4F)$ excited d levels situated below the CB of ZGO its energy is transferred to a neighboring antisite defect created by the neutral association of a Ga^{3+} ion at a Zn^{2+} site (Ga°_{Zn}) and a Zn^{2+} ion at a Ga^{3+} site (Zn'_{Ga}). Based on the specific and close location of a pair of Ga°_{Zn} and Zn'_{Ga} defects relative to the emitting Cr_{N2}^{3+} ion, the antisite defect creates a local electric field that constitutes the driving force for charge separation. As the two complementary antisite defects become neutralized, the electric field at the origin of the charge separation is suppressed. The reverse process (detrapping) is then triggered by thermal activation leading to an excited $(Cr^{3+})^\star$ followed by the emission from its $^2E(^2G)$ excited state. This kind of localized mechanism can only exist in PerL materials where the luminescent ion and the trapping defects are in close proximity to each other. This is what Pan et al. observed and described as a tunneling mechanism in parent material ZGGO:Cr [11].

Finally, in a third type of systems, infrared light is the excitation source and a two-photon absorption mechanism takes place before charging the PerL material. Two-photon absorption efficiency is reputed to low but is partly compensated by an efficient absorption of the PerL material across band gap or *via* charge transfer, f–d or d–d absorption bands. In practical, the impinging light can be up-converted through various means. A tandem of up-converting lanthanide ions like Yb^{3+} and Er^{3+} can be directly introduced into the host matrix of the PerL material [184]. Alternatively, an up-converting material can be added as a second constituent of the nanoagent and located in the vicinity of the PerL material in the form of a core–shell structure or as a dual constituent in an implant for instance [144]. Finally Liu et al. unveiled the
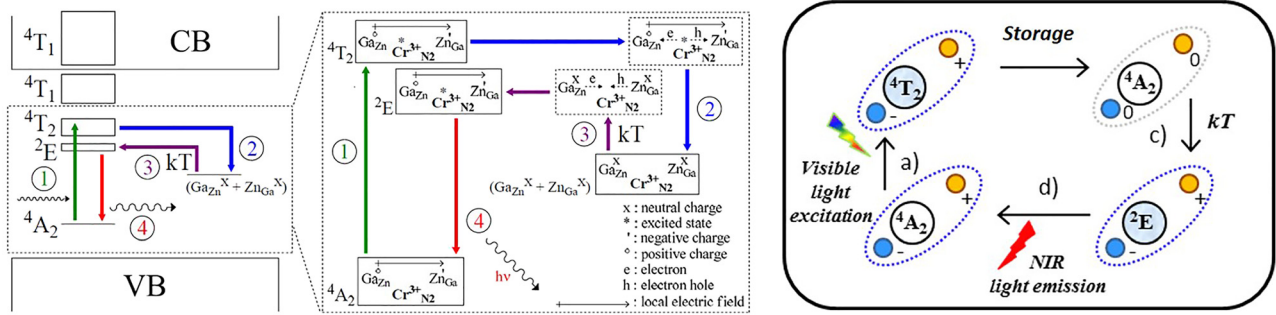
Figure 6: Mechanism of charge trapping and detrapping after a visible excitation leading to long-lasting phosphorescence in ZGO:Cr. Reproduced with permissions from [14, 183].

unexpected and exciting new concept of direct up-conversion excitation of a PerL material in Zn_3Ga_4-Ge_2O_{13}:Cr^{3+}. This rare property of ZGGO:Cr to be charged by 700 nm, 808 nm or 980 nm laser diode revealed an up-conversion trap filling process involving two photons as displayed in mechanism (III) of Figure 5 [185]. To our knowledge the same kind of up-conversion charging has been reported in only one other PerL material to date: LGO:Cr [186]. Such a rare mechanism should however not be mistaken with the use of infrared light as the optical stimulation source of luminescence as in the case of dosimetry materials. Interestingly two also rare cases of PerL materials "re-charged" by optical stimulation (mechanisms (b) and (b') in Figure 5) have been revealed to date. On the one hand Liu et al. reported in UV-pre-irradiated LGO:Cr that Cr^{3+} PerL emission at 716 nm can be repeatedly stimulated with a visible or NIR light according to (b) type mechanism (Figure 5) [187]. On the other hand Sharma et al. revealed the property of optically-stimulated PerL in ZGO:Cr, described as a (b') type mechanism (Figure 5) [188]. In that case ZGO:Cr is charged by visible light according to mechanism (II) by which the free carriers get trapped at very deep defects. A 980 nm optical stimulation enables the detrapping from the deep traps and the re-trapping of the charges to medium-deep traps responsible for PerL. Hence, after a visible pre-excitation, an infrared excitation enables to activate PerL again.

2.2.2 Application to PerL-mediated PDT

In most of the cases of PerL-mediated PDT, the nanoagent comprises both the PerL material and the PS molecule in proximity to each other so that PerL is efficiently transferred to the PS. An e*x situ* excitation of such a nanoagent, i.e. *outside* and *before* it enters the biological medium, would forbid any spatio-temporal control of the PDT activity, possibly resulting in the destruction of healthy tissues located along the way of the nanoagent towards the targeted

cells. Hence only one example is reported where PerLNPs are pre-irradiated with UV, before incubation with human breast cancer cells. In this example, Ramirez et al. tested the intrinsic photosensitizing potential of ZGO:Cr [189]. While inactive when PEG-conjugated, OH-functionalized ZGO:Cr nanoparticles are internalized by human breast cancer cells and then present a certain PDT effect (Table 1). Apart from this unique example, all the reported experiments of PerL-mediated PDT carry out the excitation of the PerL material *in situ*. Although UV chargeable materials constitute the vast majority of the PerL materials, examples of PerL-mediated PDT where UV light was used as the excitation source are scarce. Since UV light can hardly penetrate living tissues, the following few examples could only constitute *in vitro* tests of feasibility. Homayoni et al. reported the preparation of SMSO:Eu^{2+},Dy^{3+} nanoparticles conjugated with PpIX as PS and covalently bonded to folic acid (FA) to improve their water dispersion [141]. They incubated the nanoparticles *in vitro* with PC3 prostate cancer cells. After 5 min UV light exposition, a 15% additional cell death was observed with PpIX-conjugated SMSO:Eu^{2+},Dy^{3+} nanoparticles as compared to PpIX alone (Table 1). This demonstrated the potential of a PerL material to prolong the excitation of a PS in PDT. A second and more potent example concerns $Zn_{1.25}Ga_{1.5}Ge_{0.25}O_4$:0.5%$Cr^{3+}$,2.5%$Yb^{3+}$,0.25%$Er^{3+}$ gallo-germanate nanoparticles, noted TD-ZGGO for "triple doped ZGGO", coated with a mesoporous silica shell (m-SiO$_2$) loaded with AlPcS as PS [151]. Wang et al. showed that cancerous HeLa cells internalized TD-ZGGO@mSiO$_2$@AlPcS nanoparticles that presented no dark cytotoxicity [151]. For the same UV light fluence (8 J cm^{-2} at 405 nm) and same PS concentration, they observed for the cancerous cells a viability of only 8% with TD-ZGGO@mSiO$_2$@AlPcS against 87% with the PS AlPcS alone (Table 1). This remarkable result was obtained by using fractionated light irradiation, which exacerbates the efficacy of [PerL material + PS] systems. Note that three days later, the viability of the cancerous cells in presence of TD-ZGGO@mSiO$_2$@AlPcS fell to 1%, as

the PerL material still passively emitted light that kept activating the PDT process. Although UV light is generally not suited for biological systems, it was used here to demonstrate the potency of [PerL material + PS] system. The system appeared especially interesting in terms of dose reduction compared to a more classical [luminescent material + PS] system, as illustrated by the comparison made between TD-ZGGO@mSiO$_2$@AlPcS and QD@mSiO$_2$@AlPcS where QD are CdSe/CdS/ZnS core–shell quantum dots [151]. While the latter are reputed to be amongst the most efficient luminescent materials, the survival rate of HeLa cells amounted to 46% with TD-ZGGO@mSiO$_2$@AlPcS against 8% with QD@mSiO$_2$@AlPcS in the same conditions of fractionated light irradiation. This experiment strikingly demonstrates the specific suitability of PerL material relative to mere luminescent or scintillating material for PS coupling. The long-lasting low-intensity light delivered by a PerL material appears very favorable to PDT efficiency in living cells. Nevertheless the use of UV light as the excitation source remains problematics for broader biological applications and the demonstration of [PerL material + PS] system excitable with different wavelengths than UV (X-ray, visible or NIR radiation) is highly desired.

For that, second generation PerL materials, i.e. for which the persistent luminescence property is induced by visible or red light, are essential. In the long-lasting phosphors family, those materials are scarce and to our knowledge only ZGO:Cr and ZGGO:Cr have been used in actual demonstrations of PerL-mediated PDT activated by visible or red light. ZGO:Cr and ZGGO:Cr can be charged through Cr^{3+} $d–d$ absorption bands, i.e. through $^4A_2$ (^4F) → $^4T_2$ (^4F), $^4A_2$ (^4F) → $^4T_1$ (^4F) and $^4A_2$ (^4F) → $^4T_1$ (^4P), peaking at 570, 420 and 290 nm, respectively in ZGO:Cr. One can therefore take advantage of the most red-shifted absorption band ($^4A_2$ (^4F) → $^4T_2$ (^4F)) and use red light to go through the tissues. PDT experiments carried out with red light shone for a few minutes onto cancerous cells or tumors in small animals led to outstanding results. With a system based on Zn$_{1.25}$Ga$_{1.5}$Ge$_{0.25}$O$_4$:0.5%Cr^{3+},2.5% Yb^{3+},0.25%Er^{3+} coupled to Ce6 inside an hydrogel tested on 4T1 murine cancer cells, Sun et al. obtained a 60% cell viability after 5 min UV irradiation that further reached down to 18% after an additional 3 min red light illumination (0.7 W cm^{-2}) [148] (Table 1). In small animal the PerL-hydrogel was intra-tumorally injected after 5 min UV pre-irradiation. Two hours after Ce6 intravenous injection, the tumor was illuminated by red light for 10 min on days 1 and 7 and was found 16 times smaller than control after 15 days [148] (Table 2). Interestingly Yang et al. tested a system without any UV pre-irradiation made of Zn$_2$Ga$_{2.98}$-Ge$_{0.75}$O$_8$:0.02Cr^{3+},0.12Bi^{3+} nanoparticles coated with a

ZnPc-loaded mesoporous silica shell [150]. A single 10 min laser irradiation at 635 nm led to an 18% viability of Hepa1-6 murine hepatoma cancer cells (Table 1) and to an 80% inhibition factor growth of a hepatoma tumor in small animal (Table 2). Further examples demonstrate the potency of ZGO:Cr and ZGGO:Cr with a simple white LED. Note that as already mentioned above, the use of several cycles (2–3) is very beneficial for PerL-mediated PDT. Hence Fan et al. co-incubated ZnGa$_{1.996}$O$_4$:Cr$_{0.004}$ nanoparticles and HPPH with U87MG human glioblastoma cells and measured an 82% cell viability after 2 min white LED irradiation against 23% after three cycles [147] (Table 1). Liu et al. prepared nanoparticles made of a temperature-responsive "waxseal" composed of oleic acid and hexadecanol that encapsulated ZnGa$_{1.99}$O$_4$:0.004Cr^{3+} nanoparticles and IR780 as PS [172]. After 5 min 808 nm laser irradiation to melt the waxseal, the viability of HeLa human cervical cancer cells dropped to 54% while an additional 5 min white LED irradiation enabled to reach a viability as low as 18% (Table 1). Tested *in vivo*, the smart system enabled a total tumor suppression in four days after two injections of PerL-PS waxseal nanoparticles followed by 15 min white LED illumination (Table 2). Finally the IT injection of hollow ZnGa$_2$O$_4$:0.0001Cr^{3+} nanoparticles conjugated with SiPc followed by a double 10 min white LED irradiation also showed a large tumor suppression effect according to Wang et al. [149] (Table 2). These many examples clearly demonstrate that red/white light, coherent as well as non-coherent, is able to efficiently kill cancer cells and result in tumor suppression with ZGO:Cr or ZGGO:Cr as PerL material.

Finally, a few interesting examples of infrared-excited [PerL + PS] systems have been described. As discussed in Section 2.2.1, a primary upconversion process must be considered. Hu et al. coupled green-emitting SAO:Eu, Dy PerL material with up-converting NYF:Yb^{3+},Tm^{3+} within a polydimethylsiloxane (PDMS) implant [144]. NYF:Yb^{3+},Tm^{3+} converted 980 nm laser illumination into UV-blue light able to charge SAO:Eu,Dy. Incubated with HT29 human colon cancer cells the implant caused a drop in cell viability to 36% after four cycles of 5 s 980 nm laser excitation (Table 1). In small animal, the treatment composed of two cycles per day led to complete tumor suppression after 15 days (Table 2). Alternatively Li et al. introduced Yb^{3+} (2.5%) and Er^{3+} (0.25%) as additional doping ions into ZGGO:Cr^{3+} nanoparticles coated by a hollow silica (h-SiO$_2$) shell [155]. A single treatment consisting in the IV injection of the UV pre-irradiated nano-agent followed by a 200 s 808 nm tumor illumination led to a halved tumor volume relative to control after 21 days. A full inhibition was achieved when h-SiO$_2$ was loaded with

doxorubicin (DOX) as chemotherapeutic agent (Table 2). Finally based on the new concept of PerL up-conversion excitation revealed in $Zn_3Ga_4Ge_2O_{13}:Cr^{3+}$ [185], Abdurahman et al. reported SiPc-conjugated $Zn_3Ga_4Ge_2O_{13}:0.3\%$ Cr^{3+} nanoparticles which, after a 10 min UV pre-irradiation led to a cell viability as low as 5% after 10 min 808 nm irradiation [173]. *In vivo* a single 808 nm laser irradiation performed 4 h after the IT injection of the UV pre-irradiated conjugates was sufficient to completely suppress the tumor at day 16 (Table 2). Note that the use of 808 nm is a large asset relative to Yb^{3+}, Er^{3+} up-converting systems that impose the use of 980 nm that causes a much more important local heating in biological systems. Furthermore, the system appeared as remarkably efficient.

Finally, a few publications report the use of X-rays for charging the PerL material in PerL-mediated PDT. Any PerL material can theoretically be activated with X-rays provided it presents a sufficiently high stopping power towards the latter. Scintillator materials are typically conceived to greatly absorb ionizing radiation due to the presence of heavy elements in their composition and a densely packed host matrix. In PDT the use of X-rays as the excitation source of the PerL bioprobe enables to tackle virtually any deep-seated tumor as the attenuation of the X-rays across a living body is limited. However, the irradiation must be kept to a minimum dose. In 2014 Ma et al. reported a first preliminary study where ZnS:Cu,Co PerLNPs conjugated with TetraBromoRhodamine-123 (TBrRh123) as PSs were incubated with PC3 human prostate cancer cells [145]. The cells viability dropped from 90% in the dark to 40% after 1 min. X-ray irradiation (2 Gy) (Table 1). Note the special asset of PerL materials compared to mere scintillating materials: in order to obtain the same cell death rate, the use of $LaF_3:Tb^{3+}$ scintillating nanoparticles would have required an X-ray dose as high as 13.2 Gy [145]. In PerL materials the afterglow continues activating PDT after the X-ray irradiation has stopped and therefore prolongs the photodynamic treating time by a great extent, which in turn allows a reduction of the X-ray irradiation time. In 2016 Homayoni et al. showed preliminary results with 270 nm-large $Sr_2MgSi_2O_7:Eu,Dy$ PerLNPs conjugated to PpIX and to FA for targeting. The nanoparticles were shown to produce singlet oxygen after X-ray irradiation and to penetrate PC3 prostate cancer cells but the authors did not provide any further quantitative data [190]. Chen et al. developed nanoparticles made of a 100 nm-diameter LGO:Cr PerL core coated with a 25 nm mesoporous silica shell loaded with NC [152]. The viability of non-small cell lung cancer H1299 cells incubated with the nanoparticles was reduced to 46.4% after 2 Gy irradiation (Table 1). The cell viability amounted 50.2 and 60.1%

when the experiment was conducted across respectively 1.6 and 2.8 cm thick pork slice demonstrating a good penetration of X-rays across the living tissues. Cetuximab, added as a targeting agent, enabled the nanoparticles to accumulate in the cancer cells *in vitro* as well as *in vivo*. *In vivo* a 6 Gy X-ray irradiation applied to the delimited area of the tumor led after seven days to a tumor size equal to 8% that of the control (Table 2) while the tissues around remained unaffected. In 2018 Song et al. prepared ZGO:Cr and W(VI) co-doped ZGO:Cr,W PerLNPs coupled to ZnPcS4 and incubated them with HeLa human cervical cancer cells on the one hand and S180 murine sarcoma cells on the other hand [146]. After 2 min. X-ray irradiation (0.09 Gy min^{-1}) the cells viability dropped to 78% with ZGO:Cr and to 48% with ZGO:Cr,W for both cell types. The addition of tungsten as codopant was proposed to improve the stopping power of the material and indeed enhanced PerL by a factor 2 due to both a better X-ray attenuation coefficient and the creation of new traps. Again, a remarkable additional drop in cells viability was observed after three cycles (23% for HeLa cells/19% for S180 cells) (Table 1). *In vivo*, injections of ZGO:Cr,W-ZnPcS4 nanoagents on days 1 and 7, followed by a low-dose irradiation (2 min at 0.09 Gy min^{-1}) delivered 4 h after their IV injection, led to the complete inhibition of the tumor growth after 16 days, whereas tumor size in controls was multiplied by 10 (Table 2). Note that the dose used here (0.36 Gy) is far below the dose used in clinical radiotherapy (typically 60–80 Gy for solid epithelial tumors [191], in fractions of 2–5 Gy each [192]). Shi et al. prepared nanoplatforms composed of mesoporous silica nanoparticles loaded with $Zn_3Ga_2GeO_8:Cr^{3+},Yb^{3+},Er^{3+}$ prepared using a silica templating method [174]. PEG was grafted at the nanoparticles surface and the nanoparticles were subsequently loaded with SiPc. When incubated with ZGGO:Cr@m-SiO$_2$@SiPc-PEG, the viability of HepG2 human hepatocellular carcinoma cells dropped to 53% after a 4 Gy X-ray irradiation (Table 1). *In vivo*, the hepatic tumors of mice were irradiated by 4 Gy 8 h after the injection of ZGGO:Cr@m-SiO$_2$@SiPc-PEG. After 14 days the bioluminescence signal of the tumor was divided by 14.7 (Table 2).

Overall the results presented here tend to show a lower efficiency *in vitro* for X-ray excited systems (around 40–50% cells viability after one cycle) relative to light-excited systems (around 20% cells viability) although the publication of Song et al. that used ZGO:Cr,W constitutes an exception with a 20% cells viability. *In vivo* the two publications of Shi et al. and Song et al. display an efficient inhibition of the tumor growth. An increased efficiency could however probably be targeted by designing a better X-ray absorbing material. For that, nanoparticles made of

scintillating materials presenting afterglow should be specifically designed. A recent attempt in that sense has been reported by Hu et al. with NYF:Tb^{3+} that presents a higher stopping power than ZGO:Cr due to its yttrium content. The results are very preliminary as the material was synthetized as a micronic powder. NYF:Tb^{3+} was combined with g-C$_3$N$_4$ (photocatalyst) to realize deep implants in order to inactivate bacteria. After 2 min. X-ray irradiation, the viabilities of bacteria Pseudomonas Aeruginosa PAO1 cells decreased to 67.1% and further to 30.9% 5 h after ceasing the irradiation (Table 1) [126].

2.3 Physical assemblages, tumor targeting and multi-modality in PerL-mediated PDT

The success of PerL-mediated PDT also strongly depends on the co-localization of the various elements at stake in the process. On the one hand the PerL material and the PS should be close to each other for an optimum energy transfer. On the other hand, the PS should produce singlet oxygen in the closest proximity to the tumor cell. More precisely the illumination of the PS by the PerL material should occur when the PS is in the closest proximity to the tumor cells.

The most straightforward mean to associate the PerL NP with the PS is the conjugation of the PS at the surface of the nanoparticle as shown in Figure 7(a). Abdurahman et al. [173] and Li et al. [155] first aminated the surface of ZGGO:Cr nanoparticles with (3-amino propyl)triethoxysilane (APTES) then linked SiPc *via* a condensation reaction between the NH$_2$ groups on the nanoparticles surface and the Cl atoms of the SiPc molecules. Similarly Song et al. [146] used APTES to aminate ZGO:Cr nanoparticles and coupled ZnPcS4 to their surface *via* electrostatic interaction. The second most widespread method is to coat the PerLNP with a layer of mesoporous silica and then load the PS into the pores, as shown

in Figure 7(b). Wang et al. [151] coated ZGGO:Cr,Yb,Er nanoparticles with a layer of mesoporous silica prepared from tetraethyl orthosilicate (TEOS) and APTES as double silane precursors following a method developed in [193] so that the porous nanoparticles have multiple amine groups on their inner and outer surfaces. AlPcS was then easily loaded by incubation overnight through electrostatic interaction. Chen et al. [152] used the same protocol for coating LGO:Cr and loaded NC as the PS [117]. Although no head-to-head comparison has been reported, the realization of mesoporous silica shells around the PerLNPs should largely increase the number of attached PS molecules to the PerLNP as compared to a mere attachment to the outer surface and therefore should result in efficiency enhancement. However the silica shell might lengthen the distance between the PerL material and the PS and hinder a possible non-radiative FRET transfer. Note the interesting concept of porous hollow PerLNPs schematized in Figure 7(c) and developed by Wang et al. [149]. The latter prepared ZGO:Cr nanoparticles around purgeable carbon spheres that led to large hollow cavity porous PerLNPs able to load both SiPc and a chemical drug (doxorubicine). Finally Shi et al. [174] reported a template synthesis of ZGGO:Cr,Yb,Er in the pores of mesoporous silica nanoparticles as schematized in Figure 7(d). This method presents a real interest for preparing efficient PerL nano-sized materials since the PerL phenomenon is largely dependent on the good crystallization of the materials. Template synthesis enables to anneal the PerL material and therefore improve its crystalline quality while constraining its size in the pores volume of silica nanoparticles.

Table 3 summarizes the sizes of the nanoparticles assemblages used to perform *in vivo* PerL-mediated PDT. Most commonly a PerL core of around 50 nm is prepared so as to conserve efficient PerL property. However the unique realization of Song et al. [146] relies on a ZGO:Cr,W core of only 15 nm diameter and still yields an efficient tumor growth inhibition.
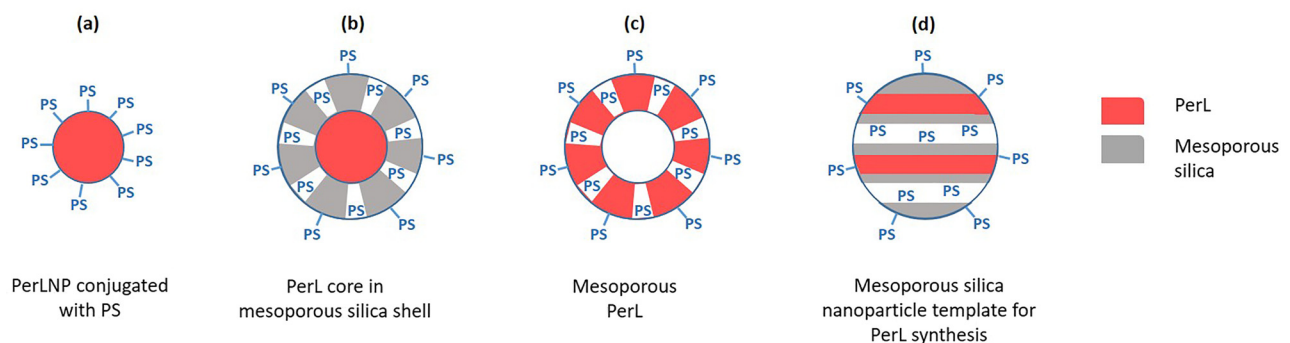
Figure 7: Variety of PS and PerLNP associations in reported examples of PerL-mediated PDT.

Table 3: Sizes of nanoparticles systems for *in vivo* PerL-mediated PDT. *Size according to TEM (hydrodynamic size according to DLS).

Author, date	PerL material	PerL synthesis method	Size of PerL core*	Shell	Size of PerL core + m-SiO$_2$*	Surface	Size of PerL core + m-SiO$_2$ + surface*
[152]	LGO:Cr	Polystyrene sphere assisted sol–gel + calcination @1000–1100 °C	100 nm	m-SiO$_2$	126 nm	PEG + cetuximab	–
[146]	ZGO:Cr,W	Hydrothermal + calcination @950 °C	15 nm (70 nm)	–	–	ZnPcS4	(78 nm)
[149]	h-ZGO:Cr	Templating over consumable carbon nanospheres (calcination @800 °C)	50 nm	–	–	–	–
[173]	ZGGO:Cr	Solvothermal + calcination @ 1000 °C	42 nm	–	–	SiPc	(163 nm)
Li et al. 2018c	ZGGO:Cr,Yb,Er	Surfactant-aided hydrothermal + calcination @ 1000 °C	(48 nm)	h-SiO$_2$	62 nm (147 nm)	CCM or LP	150 nm (176 nm)
Shi et al. 2020	ZGGO:Cr,Yb,Er	Templating in m-SiO$_2$ NPs + calcination @ 850 °C	–	–	100 nm	PEG	140 nm
[150]	ZGGO:Cr,Bi	Hydrothermal + calcination @ 750–800 °C	58 nm	m-SiO$_2$	73 nm	–	–

Concerning the localization of the PS at the tumor site, two possible strategies have been explored. On the one hand some authors relied on the EPR effect by which ZGO:Cr,W [146], ZGGO:Cr,Yb,Er [174], or ZGO:Cr,Bi [150] PerLNPs with or without a mesoporous silica shell passively accumulated into tumors. On the other hand Chen et al. [152] prepared LGO:Cr nanoparticles embedded in mesoporous silica shells conjugated with cetuximab, an anti-epidermal growth factor receptor (EGFR) antibody able to target non-small cell lung cancer tumors implanted into the lungs of rodent models. They showed a clear accumulation in the lung tumors whereas the cell uptake was minimum for particles without cetuximab. Li et al. [155] used the smart delivery system of cancer cell membrane (CCM) and realized a biomimetic nanoplatform able to target unvascularized metastasis of an orthotopic breast tumor model. The nanoplatform was composed of ZGGO:Cr,Yb,Er nanoparticles conjugated to SiPc in mesoporous silica co-loaded with doxorubicin and then coated with 4T1 cancer cell membranes.

In order to address the important question of long-lasting retention of the PerLNPs at the tumor site, a few authors proposed the interesting concept of implants. Implants are solid or solidified materials inserted into or at proximity of the cancerous tumor. The reported implants included the PerL material prepared beforehand as a nanometric or micrometric powder. Hu et al. prepared a few millimeter-large polydimethylsiloxane (PDMS) solid implant containing the green-emitting long-lasting phosphor SAO:Eu,Dy and implanted it subcutaneously onto the tumor surface of a mouse (Figure 8(a)) [144]. In order to tackle deeper tumors and to avoid the invasive

transplantation of a solid implant, others prepared syringeable materials in the form of a liquid or a gel injected intra-tumorally to the small animal. Fan et al. prepared implants made of poly(lactic-co-glycolic acid) (PLGA) and *N*-methylpyrrolidone (NMP) containing ZGO:Cr (Figure 8(b)) [147]. Such an oleosol turned from liquid to solid by quickly forming a precipitate upon water contact or in physiological environment. Sun et al. realized a biocompatible Ca^{2+} alginate hydrogel loaded with ZGGO:Cr,Yb,Er (Figure 8(c)) [148]. They carefully adjusted Ca^{2+} and ZGGO:Cr,Yb,Er to alginate ratio to reach a compromise between hardness and viscosity. Implants present several valuable advantages over free nanoparticles. First and foremost they guarantee a higher brightness for the PerL material since they passivate the surface of the PerL particles and decrease the rate of non-radiative de-excitations (Figure 9(a) and (b)) [144, 147]. Furthermore they enable the loading of micrometric powders which are much more efficient PerL materials than nanoparticles due to a better crystalline quality (Figure 9(c)) [144, 148]. Secondly, the localization of the PerL material at the tumor site is quasi-permanent and any leakage towards the surrounding tissues or bloodstream is avoided. Finally, a large diversity of theranostic agent regardless their hydrophilic or hydrophobic characteristics can be co-embedded in the implant. For example Hu et al., together with SAO:Eu,Dy, embedded an up-converting material (NYF:Yb,Er) as well as CaO$_2$ to overcome the hypoxia condition of the tumor [144]. Compared to a mere tumor size reduction of 50% that of the control after 15 days, the addition of CaO$_2$ led to the total suppression of the tumor (Table 2). Note that two options exist concerning

the loading or not of the PS within the implant. Hu et al. co-loaded RB in addition to the PerL material, which guaranteed the most efficient energy transfer from PerL to PS while the PDT activity is limited to the implant surface and therefore to the destruction of the membrane of cells appressed. Alternatively Fan et al. [147] and Sun et al. [148] embedded only the long-lasting phosphor in the implants while the PS was separately injected (intravenously) at convenient timings. In this option the PS is closer to the cells to be killed. This option led to very efficient tumor destruction within protocols presenting a limited illumination (two times 15 min white LED [147] or 10 min red light with UV pre-irradiated implant [148]).

Finally, the exciting potential of multimodality in PerL-mediated PDT systems has been explored. Interestingly most of the PerLNPs used in the reported examples possessed a PerL imaging capacity so that a theranostic use of the nano-agents was demonstrated. In all cases of *in vivo* PerL-mediated PDT except when the PerL material emits in the green [144], LGO:Cr, ZGO:Cr and ZGGO:Cr emit a luminescence above 650 nm. This red/NIR radiation easily goes through the tissues so that autofluorescence-free PerL imaging is possible *in vivo*. Chen et al. [152] and Shi et al. [174] underscored this primary role of LGO:Cr nanoparticles and ZGGO:Cr,Yb,Er nanoparticles, respectively, that enabled them to navigate the X-ray irradiation within

the tumor area with imaging guidance. Once the authors had tracked the nanoparticles in the tumor area with the help of a mild X-ray irradiation, a more intense X-ray irradiation was applied to the delimited area to implement PDT. The imaging ability of the PerL material was also advantageously exploited in the smart example of the "wax-sealed" theranostic nanoplatform developed by Liu et al. [172] (Figure 10(a)). ZGO:Cr and the PS IR780 were encapsulated in temperature-responsive wax-seal nanoparticles that prevent the premature initiation of PDT. The nanoparticles tracking by PerL imaging enabled the authors to trigger at the desired moment the photothermal excitation that melted down the wax-seals and enabled the contact of PerLNPs and PS with oxygen in the small animal body. On the other hand a few authors demonstrated the successful implementation of bi-therapeutic nano-agents. To couple PDT with chemotherapy, they synthesized hollow structures like hollow ZGO:Cr [149] (Figure 10(b)) or h-SiO$_2$-coated ZGGO:Cr,Yb,Er [155] (Figure 10(c)), which enabled the loading of the anti-cancer drug doxorubicin. Doxorubicin-loaded h-SiO$_2$-coated ZGGO:Cr,Yb,Er reduced the number of metastatic nodules in mouse from 48 to 16, without irradiation, and further to 2 after an 808 nm laser irradiation had been applied for 200 s to trigger PerL-mediated PDT, hence proving a synergetic effect of chemotherapy and PDT.
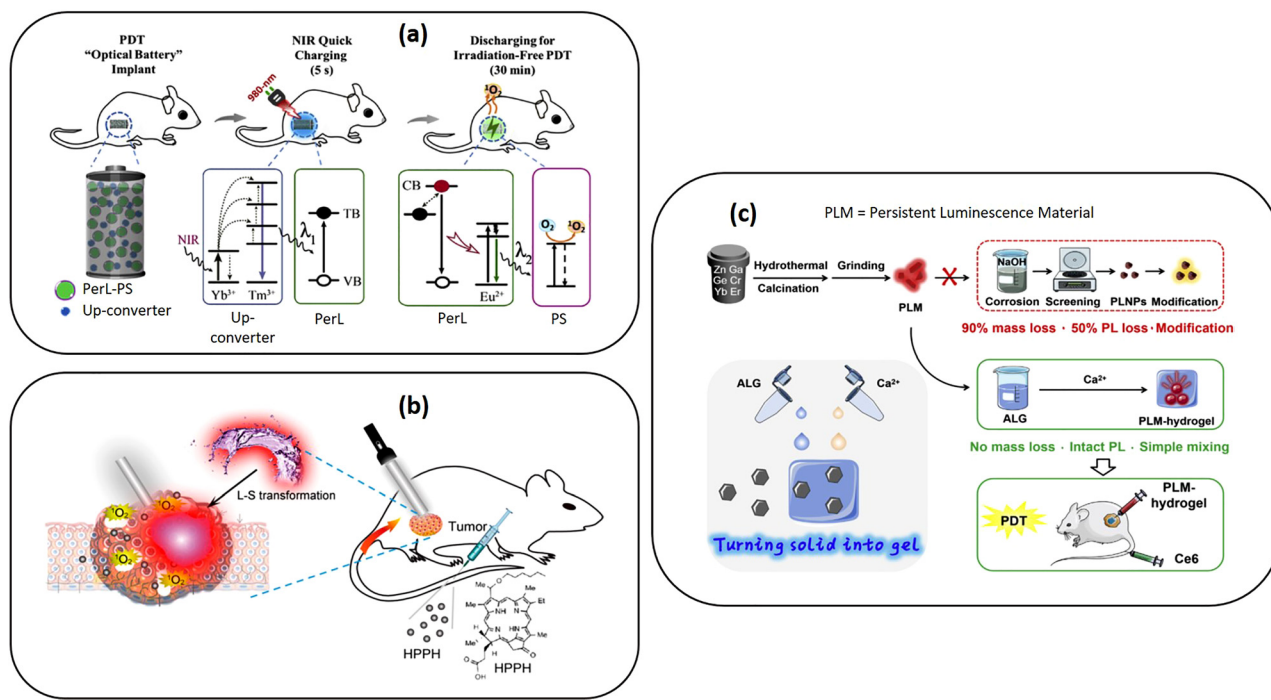
Figure 8: Examples of implants implementing PerL-mediated PDT: (a) SAO:Eu,Dy-containing PDMS solid implant [144] (b) ZGO:Cr-containing PLGA-NMP oleosol [147] and (c) ZGGO:Cr,Yb,Er-containing Ca^{2+} alginate hydrogel [148]. Reproduced with permissions from [144, 147, 148].
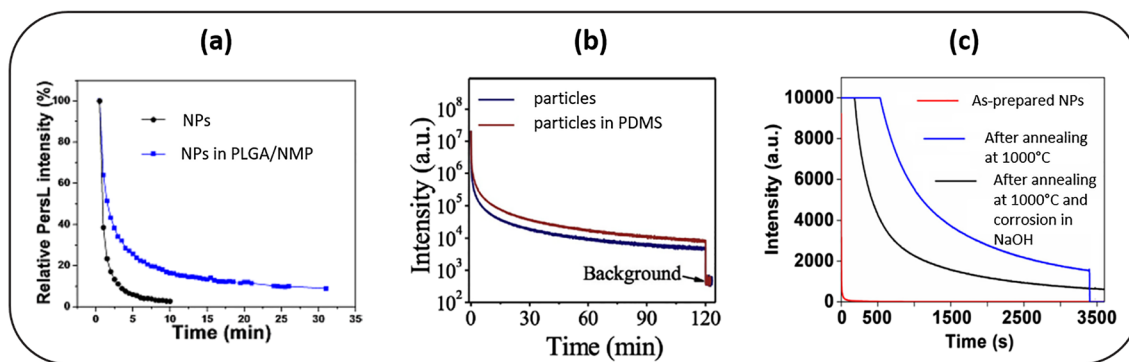
Figure 9: Persistent luminescence decay curves of (a) ZGO:Cr nanoparticles in water as compared to ZGO:Cr nanoparticles in PLGA/NMP after 2 min white LED charging [147] (b) NYF:Yb,Tm/SAO:Eu,Dy particles (mass ratio 1:10) with and without the protection of PDMS after 5 s 980 nm laser charging [144] (c) ZGGO:Cr,Yb,Er particles prepared by hydrothermal synthesis after 5 min 254 nm UV lamp charging [148]. Reproduced with permissions from [144, 147, 148].
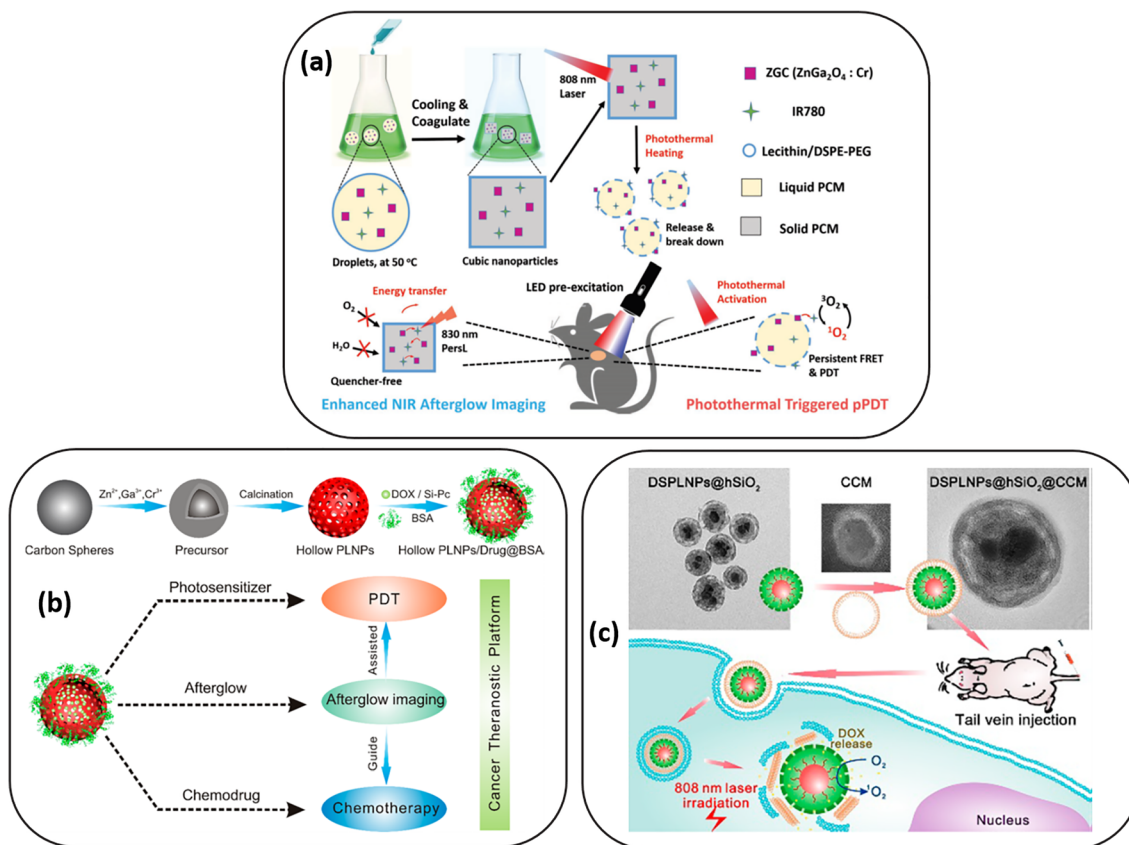
Figure 10: Examples of multi-modal realizations where PerL-mediated PDT is coupled to (a) PerL imaging [172] (b) PerL imaging and chemotherapy [149] (c) chemotherapy [155]. Reproduced with permissions from [149, 155, 172].

3 Conclusion and future directions

PDT is recognized as a wonderful tool for killing cancerous cells with the spatio-temporal control that light irradiation can provide. Unfortunately, the technique is severely limited by the poor penetration of light in living tissues. PDT against deep-seated tumors therefore remains a challenge. To overcome the weak penetration of an external light excitation, mediating nano-agents serving as internal lights are being developed to excite the photosensitizers. Amongst them PerL materials represent a unique class of mediators. Recently developed as nanoprobes enabling autofluorescence-free

in vivo imaging in small animals, they have now appeared in numerous examples of PerL-mediated PDT. In most of the reported examples, ZGO:Cr or ZGGO:Cr are used as the PerL material, which conveniently enables the double modality of PDT and PerL imaging. To realize efficient PerL-mediated PDT, authors have developed ingenious ways to couple the PerL material (SAO:Eu,Dy, ZnS:Cu,Co, LGO:Cr, ZGO:Cr, ZGGO:Cr, NYF:Tb) with a photosensitizer such as RB, HPPH, a phthalocyanine or a chlorin. The spectral match of the PerL material with the PS has often been found sub-optimal. Nevertheless, the results in terms of cell killing *in vitro* and most importantly in terms of tumor suppression *in vivo* in small animals are impressive. While the PS activity starts with the luminescence produced during the external excitation of the systems, the ROS production and cell killing effect is prolonged with the PerL emitted after the external excitation has ceased. The long-lasting and low fluence light delivery provided by the PerL material appears as particularly suited for a metronomic PDT activity. Apart from the conjugation of the PS at the surface of the PerLNPs, systems based on mesoporous silica nanoparticles appear as particularly suited to couple the PerL material with the PS. They enable a more important PS loading around the PerL NP but also permit the coupling of a second therapeutic modality (chemotherapy) that proved synergetic with PDT. Whether coated or not with a mesoporous silica shell, PerLNPs have also been successfully designed with various surface agents (antibody, lecithin, liposome, biomimetic cancer cell membrane…) for an active targeting of the tumors. For the most efficient targeting effect towards cancerous tumors, implants have been developed as a valuable alternative to nanoparticles. As far as the PerL material is concerned, implants lead to an enhancement of the PerL intensity due to a decreased number of non-radiative recombinations caused by a better crystallinity and a decreased surface area. Finally, it is worth mentioning the large versatility in the PerL materials charging. The efficacy of PerL-mediated PDT systems has been proved with a large diversity of excitation wavelength, ranging from the infrared (980 and 808 nm) to visible as well as X-rays. The use of laser is not compulsory and white LEDs were proved sufficient to eradicate mice tumors in several examples. X-ray excited PerL-mediated PDT nevertheless appears as a particularly promising modality for aiming at deep-seated tumor eradication in bigger animals or humans. A few examples already show positive results in mice but an improvement of the performance seems possible if new PerL materials with higher effective atomic number for example are developed specifically for X-ray excited persistent luminescence. Furthermore a new interest

for UV-emitting PerL phosphor for PDT mediation has recently emerged [194]. Provided the phosphors can be prepared as nanomaterials, the latter could give rise to new and more efficient PerL + PS couples.

The present review has presented *in vitro* and *in vivo* demonstrations of PDT efficiency of systems associating a PerL material with a PS. In that sense, the variety of realizations related here tends to prove efficacy and underlines the potential interest of such an association for future use. Toxicity has been studied for ZGO and ZGGO PerL NPs [175, 195] as well as hematocompatibility [196] and elimination pathways [197] as summarized in the review paper of Wu et al. [13] that presents encouraging results. Note that a size reduction of the PerL NPs, as realized in imaging examples [163], can be envisaged to permit a urinary eviction and prevent possible long-term toxicity.

Overall we can regret that the evaluation of the PerL + PS systems is almost exclusively based on cell death rate or tumor size measurement while the efficiency of several intermediate steps remains obscure. Studies concerning underlying mechanisms appear highly needed to tackle a few unanswered questions and would probably be very fruitfull in terms of efficacy enhancement. For example, the PerL efficiency of each material in its form of use could be evaluated as recommended by Van der Heggen et al. [198]. Further, the energy transfer mechanisms from the PerL material to the PS remain largely overlooked while this step is crucial as far as the system efficiency is concerned.

References

[1] T. Matsuzawa, Y. Aoki, N. Takeuchi, and Y. Murayama, "New long phosphorescent phosphor with high brightness, $SrAl_2O_4:Eu^{2+},Dy^{3+}$," *J. Electrochem. Soc.*, vol. 143, no. 8, pp. 2670–2673, 1996.

[2] Y. Lin, Z. Tang, Z. Zhang, X. Wang, and J. Zhang, "Preparation of a new long afterglow blue-emitting $Sr_2MgSi_2O_7$-based photoluminescent phosphor," *J. Mater. Sci. Lett.*, vol. 20, no. 16, pp. 1505–1506, 2001.

[3] Y. Lin, Z. Tang, and Z. Zhang, "Preparation of long-afterglow $Sr_4Al_{14}O_{25}$-based luminescent material and its optical properties," *Mater. Lett.*, vol. 51, no. 1, pp. 14–18, 2001.

[4] Y. Lin, Z. Tang, Z. Zhang, and C. W. Nan, "Luminescence of Eu^{2+} and Dy^{3+} activated $R_3MgSi_2O_8$-based (R = Ca, Sr, Ba) phosphors," *J. Alloys Compd.*, vol. 348, nos 1–2, pp. 76–79, 2003.

[5] Q. L. de Chermont, C. Chaneac, J. Seguin, et al., "Nanoprobes with near-infrared persistent luminescence for in vivo imaging [Article]," *Proc. Natl. Acad. Sci. USA*, vol. 104, no. 22, pp. 9266–9271, 2007.

[6] A. Bessiere, A. Lecointre, K. R. Priolkar, and D. Gourier, "Role of crystal defects in red long-lasting phosphorescence of $CaMgSi_2O_6$:Mn diopsides," *J. Mater. Chem.*, vol. 22, no. 36, pp. 19039–19046, 2012.

[7] A. Lecointre, A. Bessiere, K. R. Priolkar, D. Gourier, G. Wallez, and B. Viana, "Role of manganese in red long-lasting phosphorescence of manganese-doped diopside for in vivo imaging," *Mater. Res. Bull.*, vol. 48, no. 5, pp. 1898–1905, 2013.

[8] T. Maldiney, A. Lecointre, B. Viana, et al., "Controlling electron trap depth to enhance optical properties of persistent luminescence nanoparticles for in vivo imaging," *J. Am. Chem. Soc.*, vol. 133, no. 30, pp. 11810–11815, 2011.

[9] T. Maldiney, A. Lecointre, B. Viana, et al., "Trap depth optimization to improve optical properties of diopside-based nanophosphors for medical imaging," in *Oxide-Based Materials and Devices III (Proceedings of SPIE)*, F. H. Teherani, D. C. Look, and D. J. Rogers, Eds., 2012.

[10] A. Bessiere, S. Jacquart, K. Priolkar, A. Lecointre, B. Viana, and D. Gourier, "$ZnGa_2O_4$:Cr^{3+}: a new red long-lasting phosphor with high brightness," *Opt. Express*, vol. 19, no. 11, pp. 10131–10137, 2011.

[11] Z. W. Pan, Y. Y. Lu, and F. Liu, "Sunlight-activated long-persistent luminescence in the near-infrared from Cr^{3+}-doped zinc gallogermanates," *Nat. Mater.*, vol. 11, no. 1, pp. 58–63, 2012.

[12] J. H. Liu, T. Lecuyer, J. Seguin, et al., "Imaging and therapeutic applications of persistent luminescence nanomaterials [Review]," *Adv. Drug Deliv. Rev.*, vol. 138, pp. 193–210, 2019.

[13] S. Wu, L. Yang, W. Ding, L. Xu, M. Yuan, and L. Zhang, "Recent advances of persistent luminescence nanoparticles in bioapplications," *Nano-Micro Lett.*, vol. 12, no. 1, pp. 1–26, 2020.

[14] T. Maldiney, A. Bessiere, J. Seguin, et al., "The in vivo activation of persistent nanophosphors for optical imaging of vascularization, tumours and grafted cells," *Nat. Mater.*, vol. 13, no. 4, pp. 418–426, 2014.

[15] N. He, Y. Jiang, L. Lei, and Y. Liu, "Background-free cell surface glycan analysis using persistent luminescence nanoparticle as an optical probe," *Anal. Biochem.*, vol. 601, p. 113780, 2020.

[16] J. L. Li, J. P. Shi, J. S. Shen, H. Z. Man, M. X. Wang, and H. W. Zhang, "Specific recognition of breast cancer cells in vitro using near infrared-emitting long-persistence luminescent $Zn_3Ga_2Ge_2O_{10}$:Cr^{3+} nanoprobes [Article]," *Nano-Micro Lett.*, vol. 7, no. 2, pp. 138–145, 2015.

[17] J. Shi, X. Sun, J. Zhu, J. Li, and H. Zhang, "One-step synthesis of amino-functionalized ultrasmall near infrared-emitting persistent luminescent nanoparticles for in vitro and in vivo bioimaging," *Nanoscale*, vol. 8, no. 18, pp. 9798–9804, 2016.

[18] J. Wang, Q. Ma, X.-X. Hu, et al., "Autofluorescence-free targeted tumor imaging based on luminous nanoparticles with composition-dependent size and persistent luminescence," *ACS Nano*, vol. 11, no. 8, pp. 8010–8017, 2017.

[19] S.-Q. Wu, C.-W. Chi, C.-X. Yang, and X.-P. Yan, "Penetrating peptide-bioconjugated persistent nanophosphors for long-term tracking of adipose-derived stem cells with superior signal-to-noise ratio," *Anal. Chem.*, vol. 88, no. 7, pp. 4114–4121, 2016.

[20] J.-M. Liu, D.-D. Zhang, G.-Z. Fang, and S. Wang, "Erythrocyte membrane bioinspired near-infrared persistent luminescence nanocarriers for in vivo long-circulating bioimaging and drug delivery," *Biomaterials*, vol. 165, pp. 39–47, 2018.

[21] T. Maldiney, B. Ballet, M. Bessodes, D. Scherman, and C. Richard, "Mesoporous persistent nanophosphors for in vivo optical bioimaging and drug-delivery," *Nanoscale*, vol. 6, no. 22, pp. 13970–13976, 2014.

[22] H. B. Chen, B. Zheng, C. Liang, et al., "Near-infrared persistent luminescence phosphors ($ZnGaO_4$)-O-2:Cr^{3+} as an accurately tracker to photothermal therapy in vivo for visual treatment [Article]," *Mater. Sci. Eng. C Mater. Biol. Appl.*, vol. 79, pp. 372–381, 2017.

[23] L.-J. Chen, S.-K. Sun, Y. Wang, C.-X. Yang, S.-Q. Wu, and X.-P. Yan, "Activatable multifunctional persistent luminescence nanoparticle/copper sulfide nanoprobe for in vivo luminescence imaging-guided photothermal therapy," *ACS Appl. Mater. Interfaces*, vol. 8, no. 48, pp. 32667–32674, 2016.

[24] L. Qin, P. Yan, C. Xie, et al., "Gold nanorod-assembled $ZnGa_2O_4$:Cr nanofibers for LED-amplified gene silencing in cancer cells," *Nanoscale*, vol. 10, no. 28, pp. 13432–13442, 2018.

[25] S.-Q. Wu, C.-X. Yang, and X.-P. Yan, "A dual-functional persistently luminescent nanocomposite enables engineering of mesenchymal stem cells for homing and gene therapy of glioblastoma," *Adv. Funct. Mater.*, vol. 27, no. 11, p. 1604992, 2017.

[26] J. P. Celli, B. Q. Spring, I. Rizvi, et al., "Imaging and photodynamic therapy: mechanisms, monitoring, and optimization," *Chem. Rev.*, vol. 110, no. 5, pp. 2795–2838, 2010.

[27] S. Gai, G. Yang, P. Yang, et al., "Recent advances in functional nanomaterials for light–triggered cancer therapy," *Nano Today*, vol. 19, pp. 146–187, 2018.

[28] X. Li, S. Lee, and J. Yoon, "Supramolecular photosensitizers rejuvenate photodynamic therapy," *Chem. Soc. Rev.*, vol. 47, no. 4, pp. 1174–1188, 2018.

[29] C. A. Robertson, D. H. Evans, and H. Abrahamse, "Photodynamic therapy (PDT): a short review on cellular mechanisms and cancer research applications for PDT," *J. Photochem. Photobiol. B Biol.*, vol. 96, no. 1, pp. 1–8, 2009.

[30] R. Wang, X. Li, and J. Yoon, "Organelle-targeted photosensitizers for precision photodynamic therapy," *ACS Appl. Mater. Interfaces*, vol. 13, no. 17, pp. 19543–19571, 2021.

[31] D. van Straten, V. Mashayekhi, H. S. de Bruijn, S. Oliveira, and D. J. Robinson, "Oncologic photodynamic therapy: basic principles, current clinical status and future directions," *Cancers*, vol. 9, no. 2, 2017.

[32] L. D. Via and S. M. Magno, "Photochemotherapy in the treatment of cancer," *Curr. Med. Chem.*, vol. 8, no. 12, pp. 1405–1418, 2001.

[33] J. R. Kanofsky, "Measurement of singlet-oxygen in vivo: progress and pitfalls," *Photochem. Photobiol.*, vol. 87, no. 1, pp. 14–17, 2011.

[34] M. T. Jarvi, M. J. Niedre, M. S. Patterson, and B. C. Wilson, "The influence of oxygen depletion and photosensitizer triplet-state dynamics during photodynamic therapy on accurate singlet oxygen luminescence monitoring and analysis of treatment dose response," *Photochem. Photobiol.*, vol. 87, no. 1, pp. 223–234, 2011.

[35] S. S. Lucky, K. C. Soo, and Y. Zhang, "Nanoparticles in photodynamic therapy," *Chem. Rev.*, vol. 115, no. 4, pp. 1990–2042, 2015.

[36] G. Jori, C. Fabris, M. Soncin, et al., "Photodynamic therapy in the treatment of microbial infections: basic principles and perspective applications," *Laser Surg. Med.*, vol. 38, no. 5, pp. 468–481, 2006.

[37] T. Dai, Y. Y. Huang, and M. R. Hamblin, "Photodynamic therapy for localized infections-State of the art," *Photodiagnosis Photodyn. Ther.*, vol. 6, nos 3-4, pp. 170–188, 2009.

[38] K. D. Winckler, "Special section: focus on anti-microbial photodynamic therapy (PDT)," *J. Photochem. Photobiol. B Biol.*, vol. 86, no. 1, pp. 43–44, 2007.

[39] P. Dharmaratne, D. N. Sapugahawatte, B. Y. Wang, et al., "Contemporary approaches and future perspectives of antibacterial photodynamic therapy (aPDT) against methicillin-resistant *Staphylococcus aureus* (MRSA): a systematic review," *Eur. J. Med. Chem.*, vol. 200, pp. 112341-1–112341-27, 2020.

[40] L. Costa, J. P. C. Tome, M. Neves, et al., "Evaluation of resistance development and viability recovery by a non-enveloped virus after repeated cycles of aPDT," *Antivir. Res.*, vol. 91, no. 3, pp. 278–282, 2011.

[41] A. Wiehe, J. M. O'Brien, and M. O. Senge, "Trends and targets in antiviral phototherapy," *Photochem. Photobiol. Sci.*, vol. 18, no. 11, pp. 2565–2612, 2019.

[42] W. F. Cheong, S. A. Prahl, and A. J. Welch, "A review of the optical-properties of biological tissues," *IEEE J. Quant. Electron.*, vol. 26, no. 12, pp. 2166–2185, 1990.

[43] J. V. Frangioni, "In vivo near-infrared fluorescence imaging," *Curr. Opin. Chem. Biol.*, vol. 7, no. 5, pp. 626–634, 2003.

[44] M. M. Kim and A. Darafsheh, "Light sources and dosimetry techniques for photodynamic therapy," *Photochem. Photobiol.*, vol. 96, no. 2, pp. 280–294, 2020.

[45] R. K. Pandey, T. J. Dougherty, and K. M. Smith, "Syntheses of hematoporphyrin dimers and trimers with ether linkages," *Tetrahedron Lett.*, vol. 29, no. 37, pp. 4657–4660, 1988.

[46] E. D. Sternberg, D. Dolphin, and C. Bruckner, "Porphyrin-based photosensitizers for use in photodynamic therapy," *Tetrahedron*, vol. 54, no. 17, pp. 4151–4202, 1998.

[47] J. Usuda, H. Kato, T. Okunaka, et al., "Photodynamic therapy (PDT) for lung cancers," *J. Thorac. Oncol.*, vol. 1, no. 5, pp. 489–493, 2006.

[48] Z. Huang, "A review of progress in clinical photodynamic therapy," *Technol. Canc. Res. Treat.*, vol. 4, no. 3, pp. 283–293, 2005.

[49] A. B. Ormond and H. S. Freeman, "Dye sensitizers for photodynamic therapy," *Materials*, vol. 6, no. 3, pp. 817–840, 2013.

[50] A. E. O'Connor, W. M. Gallagher, and A. T. Byrne, "Porphyrin and nonporphyrin photosensitizers in oncology: preclinical and clinical advances in photodynamic therapy," *Photochem. Photobiol.*, vol. 85, no. 5, pp. 1053–1074, 2009.

[51] J. M. S. Lopes, J. R. T. Reis, A. E. H. Machado, et al., "Influence of the meso-substituents on the spectral features of free-base porphyrin," *Spectrochim. Acta Mol. Biomol. Spectrosc.*, vol. 238, pp. 118389-1–118389-10, 2020.

[52] S. K. Pushpan, S. Venkatraman, V. G. Anand, et al., "Porphyrins in photodynamic therapy – a search for ideal photosensitizers," *Curr. Med. Chem. Anti Canc. Agents*, vol. 2, no. 2, pp. 187–207, 2002.

[53] D. A. Bellnier, W. R. Greco, H. Nava, G. M. Loewen, A. R. Oseroff, and J. D. Thomas, "Mild skin photosensitivity in cancer patients following injection of photochlor (2-[1-hexyloxyethyl]-2-devinyl pyropheophorbide-a; HPPH) for photodynamic therapy," *Canc. Chemother. Pharmacol.*, vol. 57, no. 1, pp. 40–45, 2006.

[54] S. Yano, S. Hirohara, M. Obata, et al., "Current states and future views in photodynamic therapy," *J. Photochem. Photobiol. C Photochem. Rev.*, vol. 12, no. 1, pp. 46–67, 2011.

[55] C. C. Leznoff and A. B. P. Lever, *Phtalocyanines, Properties and Applications*, vol. 2, New York, VCH Publishers, 1992.

[56] X. Li, B.-D. Zheng, X.-H. Peng, et al., "Phthalocyanines as medicinal photosensitizers: developments in the last five years," *Coord. Chem. Rev.*, vol. 379, pp. 147–160, 2019.

[57] S. H. Mousavi, M. Tavakkol-Afshari, A. Brook, and I. Jafari-Anarkooli, "Direct toxicity of Rose Bengal in MCF-7 cell line: role of apoptosis," *Food Chem. Toxicol.*, vol. 47, no. 4, pp. 855–859, 2009.

[58] W. P. Fan, P. Huang, and X. Y. Chen, "Overcoming the Achilles' heel of photodynamic therapy [Review]," *Chem. Soc. Rev.*, vol. 45, no. 23, pp. 6488–6519, 2016.

[59] Y. Shen, A. J. Shuhendler, D. Ye, J.-J. Xu, and H.-Y. Chen, "Two-photon excitation nanoparticles for photodynamic therapy," *Chem. Soc. Rev.*, vol. 45, no. 24, pp. 6725–6741, 2016.

[60] J. Schmitt, V. Heitz, A. Sour, et al., "Diketopyrrolopyrrole-porphyrin conjugates with high two-photon absorption and singlet oxygen generation for two-photon photodynamic therapy," *Angew. Chem. Int. Ed.*, vol. 54, no. 1, pp. 169–173, 2015.

[61] T. T. Zhao, X. Q. Shen, L. Li, et al., "Gold nanorods as dual photo-sensitizing and imaging agents for two-photon photodynamic therapy," *Nanoscale*, vol. 4, no. 24, pp. 7712–7719, 2012.

[62] T. J. Dougherty, G. Lawrence, J. H. Kaufman, D. Boyle, K. R. Weishaupt, and A. Goldfarb, "Photoradiation in the treatment of recurrent breast carcinoma," *J. Natl. Cancer Inst.*, vol. 62, no. 2, pp. 231–237, 1979.

[63] T. S. Mang, "Lasers and light sources for PDT: past, present and future," *Photodiagnosis Photodyn. Ther.*, vol. 1, no. 1, pp. 43–48, 2004.

[64] M. Megna, G. Fabbrocini, C. Marasca, and G. Monfrecola, "Photodynamic therapy and skin appendage disorders: a review," *Skin Appendage Disorders*, vol. 2, nos 3–4, pp. 166–176, 2016.

[65] F. J. Civantos, B. Karakullukcu, M. Biel, et al., "A review of photodynamic therapy for neoplasms of the head and neck," *Adv. Ther.*, vol. 35, no. 3, pp. 324–340, 2018.

[66] H. Ikeda, S. Ohba, K. Egashira, and I. Asahina, "The effect of photodynamic therapy with talaporfin sodium, a second-generation photosensitizer, on oral squamous cell carcinoma: a series of eight cases," *Photodiagnosis Photodyn. Ther.*, vol. 21, pp. 176–180, 2018.

[67] K. Moghissi, "Endoscopic photodynamic therapy (PDT) for oesophageal cancer," *Photodiagnosis Photodyn. Ther.*, vol. 3, no. 2, pp. 93–95, 2006.

[68] H. Wu, T. Minamide, and T. Yano, "Role of photodynamic therapy in the treatment of esophageal cancer," *Dig. Endosc.*, vol. 31, no. 5, pp. 508–516, 2019.

[69] G. Shafirstein, A. Battoo, K. Harris, et al., "Photodynamic therapy of non-small cell lung cancer narrative review and future directions," *Ann. Am. Thor. Soc.*, vol. 13, no. 2, pp. 265–275, 2016.

[70] N. Yavari, S. Andersson-Engels, U. Segersten, and P. U. Malmstrom, "An overview on preclinical and clinical experiences with photodynamic therapy for bladder cancer," *Can. J. Urol.*, vol. 18, no. 4, pp. 5778–5786, 2011.

[71] Y. Matoba, K. Banno, I. Kisu, and D. Aoki, "Clinical application of photodynamic diagnosis and photodynamic therapy for gynecologic malignant diseases: a review," *Photodiagnosis Photodyn. Ther.*, vol. 24, pp. 52–57, 2018.

[72] G. Shafirstein, D. Bellnier, E. Oakley, et al., "Interstitial photodynamic therapy-A focused review," *Cancers*, vol. 9, no. 2, pp. 12-1–12-14, 2017.

[73] A. Claes, A. J. Idema, and P. Wesseling, "Diffuse Glioma growth: a Guerilla war," *Acta Neuropathol.*, vol. 114, no. 5, pp. 443–458, 2007.

[74] S. W. Cramer and C. C. Chen, "Photodynamic therapy for the treatment of glioblastoma," *Front. Surg.*, vol. 6, pp. 81-1–81-11, 2020.

[75] C. Heckl, M. Aumiller, A. Ruhm, R. Sroka, and H. Stepp, "Fluorescence and treatment light monitoring for interstitial photodynamic therapy," *Photochem. Photobiol.*, vol. 96, no. 2, pp. 388–396, 2020.

[76] H. Stepp and W. Stummer, "5-ALA in the management of malignant glioma," *Laser Surg. Med.*, vol. 50, no. 5, pp. 399–419, 2018.

[77] E. Oakley, D. Bellnier, A. Hutson, et al., "Irradiance, Photofrin® dose and initial tumor volume are key predictors of response to interstitial photodynamic therapy of locally advanced cancers in translational models," *Photochem. Photobiol.*, vol. 96, no. 2, pp. 397–404, 2020.

[78] D. Bechet, F. Auger, P. Couleaud, et al., "Multifunctional ultrasmall nanoplatforms for vascular-targeted interstitial photodynamic therapy of brain tumors guided by real-time MRI," *Nanomed. Nanotechnol. Biol. Med.*, vol. 11, no. 3, pp. 657–670, 2015.

[79] J. Akimoto, S. Fukami, T. Suda, et al., "First autopsy analysis of the efficacy of intra-operative additional photodynamic therapy for patients with glioblastoma," *Brain Tumor Pathol.*, vol. 36, no. 4, pp. 144–151, 2019.

[80] H. Liu, Y. Yang, A. Wang, M. Han, W. Cui, and J. Li, "Hyperbranched polyglycerol-doped mesoporous silica nanoparticles for one- and two-photon activated photodynamic therapy," *Adv. Funct. Mater.*, vol. 26, no. 15, pp. 2561–2570, 2016b.

[81] N. T. Chen, K. C. Tang, M. F. Chung, et al., "Enhanced plasmonic resonance energy transfer in mesoporous silica-encased gold nanorod for two-photon-activated photodynamic therapy," *Theranostics*, vol. 4, no. 8, pp. 798–807, 2014.

[82] K. Turcheniuk, V. Turcheniuk, C.-H. Hage, et al., "Highly effective photodynamic inactivation of E. coli using gold nanorods/SiO₂ core–shell nanostructures with embedded verteporfin," *Chem. Commun.*, vol. 51, no. 91, pp. 16365–16368, 2015.

[83] T. Zhao, K. Yu, L. Lin, et al., "Gold nanorod enhanced two-photon excitation fluorescence of photosensitizers for two-photon imaging and photodynamic therapy," *ACS Appl. Mater. Interfaces*, vol. 6, no. 4, pp. 2700–2708, 2014.

[84] S. S. Cui, D. Y. Yin, Y. Q. Chen, et al., "In vivo targeted deep-tissue photodynamic therapy based on near-infrared light triggered upconversion nanoconstruct," *ACS Nano*, vol. 7, no. 1, pp. 676–688, 2013.

[85] N. M. Idris, M. K. Gnanasammandhan, J. Zhang, P. C. Ho, R. Mahendran, and Y. Zhang, "In vivo photodynamic therapy using upconversion nanoparticles as remote-controlled nanotransducers," *Nat. Med.*, vol. 18, no. 10, pp. 1580–U1190, 2012.

[86] S. Jin, L. J. Zhou, Z. J. Gu, et al., "A new near infrared photosensitizing nanoplatform containing blue-emitting up-conversion nanoparticles and hypocrellin A for photodynamic therapy of cancer cells," *Nanoscale*, vol. 5, no. 23, pp. 11910–11918, 2013.

[87] K. Liu, X. M. Liu, Q. H. Zeng, et al., "Covalently assembled NIR nanoplatform for simultaneous fluorescence imaging and photodynamic therapy of cancer cells," *ACS Nano*, vol. 6, no. 5, pp. 4054–4062, 2012.

[88] C. Wang, L. Cheng, Y. M. Liu, et al., "Imaging-guided pH-sensitive photodynamic therapy using charge reversible upconversion nanoparticles under near-infrared light," *Adv. Funct. Mater.*, vol. 23, no. 24, pp. 3077–3086, 2013.

[89] C. Wang, H. Q. Tao, L. Cheng, and Z. Liu, "Near-infrared light induced in vivo photodynamic therapy of cancer based on upconversion nanoparticles," *Biomaterials*, vol. 32, no. 26, pp. 6145–6154, 2011.

[90] H. J. Wang, Z. Y. Liu, S. Wang, et al., "MC540 and upconverting nanocrystal coloaded polymeric liposome for near-infrared light-triggered photodynamic therapy and cell fluorescent imaging," *ACS Appl. Mater. Interfaces*, vol. 6, no. 5, pp. 3219–3225, 2014.

[91] C. N. Yang, Q. L. Liu, D. C. He, N. Na, Y. L. Zhao, and J. Ouyang, "Dual-modal imaging and photodynamic therapy using upconversion nanoparticles for tumor cells," *Analyst*, vol. 139, no. 24, pp. 6414–6420, 2014.

[92] Z. X. Zhao, Y. N. Han, C. H. Lin, et al., "Multifunctional core-shell upconverting nanoparticles for imaging and photodynamic therapy of liver cancer cells," *Chem. Asian J.*, vol. 7, no. 4, pp. 830–837, 2012.

[93] A. G. Zhou, Y. C. Wei, B. Y. Wu, Q. Chen, and D. Xing, "Pyropheophorbide A and c(RGDyK) comodified chitosan-wrapped upconversion nanoparticle for targeted near-infrared photodynamic therapy," *Mol. Pharm.*, vol. 9, no. 6, pp. 1580–1589, 2012.

[94] H. S. Qian, H. C. Guo, P. C.-L. Ho, R. Mahendran, and Y. Zhang, "Mesoporous-silica-coated up-conversion fluorescent nanoparticles for photodynamic therapy," *Small*, vol. 5, no. 20, pp. 2285–2290, 2009.

[95] A. Borodziuk, P. Kowalik, M. Duda, et al., "Unmodified Rose Bengal photosensitizer conjugated with NaYF4:Yb,Er upconverting nanoparticles for efficient photodynamic therapy," *Nanotechnology*, vol. 31, no. 46, p. 465101, 2020.

[96] G. Tian, Z. Gu, L. Zhou, et al., "Mn²⁺ dopant-controlled synthesis of NaYF₄:Yb/Er upconversion nanoparticles for in vivo imaging and drug delivery," *Adv. Mater.*, vol. 24, no. 9, pp. 1226–1231, 2012.

[97] J. Dong and J. I. Zink, "Light or heat? The origin of cargo release from nanoimpeller particles containing upconversion nanocrystals under IR irradiation," *Small*, vol. 11, no. 33, pp. 4165–4172, 2015.

[98] X. F. Chen, J. B. Song, X. Y. Chen, and H. H. Yang, "X-ray-activated nanosystems for theranostic applications," *Chem. Soc. Rev.*, vol. 48, no. 11, pp. 3073–3101, 2019.

[99] B. Cline, I. Delahunty, and J. Xie, "Nanoparticles to mediate X-ray-induced photodynamic therapy and Cherenkov radiation photodynamic therapy," *WIREs Nanomed. Nanobiotechnol.*, vol. 11, no. 2, p. e1541, 2019.

[100] W. P. Fan, W. Tang, J. Lau, et al., "Breaking the depth dependence by nanotechnology-enhanced X-ray-excited deep cancer theranostics," *Adv. Mater.*, vol. 31, no. 12, pp. 1806381-1–1806381-32, 2019.

[101] Z. Gadzhimagomedova, Z. Peter, O. Kit, D. Kirsanova, and A. Soldatov, "Nanocomposites for X-ray photodynamic therapy," *Int. J. Mol. Sci.*, vol. 21, no. 11, p. 4004, 2020.

[102] L. Larue, A. Ben Mihoub, Z. Youssef, et al., "Using X-rays in photodynamic therapy: an overview," *Photochem. Photobiol. Sci.*, vol. 17, no. 11, pp. 1612–1650, 2018.

[103] T. Liu, K. Yang, and Z. Liu, "Recent advances in functional nanomaterials for X-ray triggered cancer therapy," *Prog. Nat. Sci. Mater. Int.*, vol. 30, no. 5, pp. 567–576, 2020.

[104] X.-D. Ren, X.-Y. Hao, H.-C. Li, K. Mei-Rong, B.-Y. Zheng, and J.-D. Huang, "Progress in the development of nanosensitizers for X-ray-induced photodynamic therapy," *Drug Discov. Today*, vol. 23, no. 10, pp. 1791–1800, 2018.

[105] M. Sivasubramanian, Y. C. Chuang, and L.-W. Lo, "Evolution of nanoparticle-mediated photodynamic therapy: from superficial to deep-seated cancers," *Molecules*, vol. 24, no. 3, p. 520, 2019.

[106] W. J. Sun, Z. J. Zhou, G. Pratx, X. Y. Chen, and H. M. Chen, "Nanoscintillator-mediated X-ray induced photodynamic therapy for deep-seated tumors: from concept to biomedical applications," *Theranostics*, vol. 10, no. 3, pp. 1296–1318, 2020.

[107] K. Yan, Y. Zhang, C. Mu, et al., "Versatile nanoplatforms with enhanced photodynamic therapy: designs and applications," *Theranostics*, vol. 10, no. 16, p. 7287, 2020.

[108] W. Parker and H. Patrocinio, *Clinical treatment planning in external photon beam radiotherapy. Radiation oncology physics: a handbook for teachers and students*, Vienna, IAEA 219, 2005.

[109] S. Söderström, E. Anders, and B. Anders, "Aspects on the optimal photon beam energy for radiation therapy," *Acta Oncol.*, vol. 38, no. 2, pp. 179–187, 1999.

[110] A. B. de González, M. Mahesh, K.-P. Kim, et al., "Projected cancer risks from computed tomographic scans performed in the United States in 2007," *Arch. Int. Med.*, vol. 169, no. 22, pp. 2071–2077, 2009.

[111] W. Chen and J. Zhang, "Using nanoparticles to enable simultaneous radiation and photodynamic therapies for cancer treatment," *J. Nanosci. Nanotechnol.*, vol. 6, no. 4, pp. 1159–1166, 2006.

[112] J. P. Scaffidi, M. K. Gregas, L. Benoit, Y. Zhang, and T. Vo-Dinh, "Activity of psoralen-functionalized nanoscintillators against cancer cells upon X-ray excitation," *ACS Nano*, vol. 5, no. 6, pp. 4679–4687, 2011.

[113] M.-H. Chen, Y.-J. Jenh, S.-K. Wu, Y.-S. Chen, N. Hanagata, and F.-H. Lin, "Non-invasive photodynamic therapy in brain cancer by use of Tb³⁺-Doped LaF₃ nanoparticles in combination with photosensitizer through X-ray irradiation: a proof-of-concept study," *Nanoscale Research Letters*, vol. 12, no. 1, pp. 1–6, 2017.

[114] F. Ahmad, X. Wang, Z. Jiang, et al., "Codoping enhanced radioluminescence of nanoscintillators for X-ray-activated synergistic cancer therapy and prognosis using metabolomics," *ACS Nano*, vol. 13, no. 9, pp. 10419–10433, 2019.

[115] I. Porosnicu, C. M. Butnaru, I. Tiseanu, et al., "Y₂O₃ nanoparticles and X-ray radiation-induced effects in melanoma cells," *Molecules*, vol. 26, no. 11, p. 3403, 2021.

[116] J. Daouk, M. Iltis, B. Dhaini, et al., "Terbium-based AGuIX-design nanoparticle to mediate X-ray-induced photodynamic therapy," *Pharmaceuticals*, vol. 14, no. 5, p. 396, 2021.

[117] H. Chen, G. D. Wang, Y.-J. Chuang, et al., "Nanoscintillator-mediated X-ray inducible photodynamic therapy for in vivo cancer treatment," *Nano Lett.*, vol. 15, no. 4, pp. 2249–2256, 2015.

[118] C. Zhang, K. Zhao, W. Bu, et al., "Marriage of scintillator and semiconductor for synchronous radiotherapy and deep photodynamic therapy with diminished oxygen dependence," *Angew. Chem. Int. Ed.*, vol. 54, no. 6, pp. 1770–1774, 2015.

[119] W. Zhang, X. Zhang, Y. Shen, et al., "Ultra-high FRET efficiency NaGdF₄: Tb³⁺-Rose Bengal biocompatible nanocomposite for X-ray excited photodynamic therapy application," *Biomaterials*, vol. 184, pp. 31–40, 2018.

[120] X. Yu, X. Liu, W. Wu, et al., "CT/MRI-guided synergistic radiotherapy and X-ray inducible photodynamic therapy using Tb-doped Gd-W-nanoscintillators," *Angew. Chem. Int. Ed.*, vol. 58, no. 7, pp. 2017–2022, 2019.

[121] W. Sun, T. Shi, L. Luo, et al., "Monodisperse and uniform mesoporous silicate nanosensitizers achieve low-dose X-ray-induced deep-penetrating photodynamic therapy," *Adv. Mater.*, vol. 31, no. 16, p. 1808024, 2019.

[122] X. Zhang, B. Lan, S. Wang, et al., "Low-dose X-ray excited photodynamic therapy based on NaLuF₄: Tb³⁺-rose bengal nanocomposite," *Bioconjugate Chem.*, vol. 30, no. 8, pp. 2191–2200, 2019.

[123] Z. Jiang, L. He, X. Yu, et al., "Antiangiogenesis combined with inhibition of the hypoxia pathway facilitates low-dose, X-ray-induced photodynamic therapy," *ACS Nano*, vol. 15, no. 7, pp. 11112–11125, 2021.

[124] L. Song, X. H. Lin, X. R. Song, et al., "Repeatable deep-tissue activation of persistent luminescent nanoparticles by soft X-ray for high sensitivity long-term in vivo bioimaging [Article]," *Nanoscale*, vol. 9, no. 8, pp. 2718–2722, 2017.

[125] G. A. Mandl, D. Van der Heggen, D. R. Cooper, et al., "On a local (de-)trapping model for highly doped Pr³⁺ radioluminescent and persistent luminescent nanoparticles," *Nanoscale*, vol. 12, no. 40, pp. 20759–20766, 2020.

[126] Y. Hu, Y. M. Yang, X. F. Zhang, et al., "X-ray-excited super-long green persistent luminescence from Tb³⁺ monodoped beta-NaYF₄," *J. Phys. Chem. C*, vol. 124, no. 45, pp. 24940–24948, 2020.

[127] D. Van der Heggen, D. R. Cooper, M. Tesson, et al., "Optically stimulated nanodosimeters with high storage capacity," *Nanomaterials*, vol. 9, no. 8, p. 1127, 2019.

[128] N. T. Blum, Y. Zhang, J. Qu, J. Lin, and P. Huang, "Recent advances in self-exciting photodynamic therapy," *Front. Bioeng. Biotechnol.*, vol. 8, p. 1136, 2020.

[129] Y. Zhang, Y. Hao, S. Chen, and M. Xu, "Photodynamic therapy of cancers with internal light sources: chemiluminescence, bioluminescence, and Cerenkov radiation," *Front. Chem.*, vol. 8, pp. 770-1–770-7, 2020.

[130] M. Yang, J. Huang, J. Fan, J. Du, K. Pu, and X. Peng, "Chemiluminescence for bioimaging and therapeutics: recent advances and challenges," *Chem. Soc. Rev.*, 2020.

[131] L. Jiang, L. Liu, F. Lv, S. Wang, and X. Ren, "Integration of self-luminesce and oxygen self-supply: a potential photodynamic therapy strategy for deep tumor treatment," *ChemPlusChem*, vol. 85, pp. 510–518, 2020.

[132] A. Pantelia, I. Daskalaki, M. C. Cuquerella, G. Rotas, M. A. Miranda, and G. C. Vougioukalakis, "Synthesis and chemiluminescent properties of amino-acylated luminol derivatives bearing phosphonium cations," *Molecules*, vol. 24, no. 21, p. 3957, 2019.

[133] D. Bartusik-Aebisher, O. Łukasz, and D. Aebisher, "Alternative methods of photodynamic therapy and oxygen consumption measurements—a review," *Biomed. Pharmacother.*, vol. 134, p. 111095, 2021.

[134] E. H. Kim, S. Park, Y. K. Kim, et al., "Self-luminescent photodynamic therapy using breast cancer targeted proteins," *Sci. Adv.*, vol. 6, no. 37, p. eaba3009, 2020.

[135] D. Fan, T. Wang, J. Hu, L. Zhou, J. Zhou, and S. Wei, "Plasmid DNA-based bioluminescence-activated system for photodynamic therapy in cancer treatment," *ChemMedChem*, vol. 16, pp. 1967–1974, 2021.

[136] T. M. Shaffer, E. C. Pratt, and J. Grimm, "Utilizing the power of Cerenkov light with nanotechnology," *Nat. Nanotechnol.*, vol. 12, no. 2, pp. 106–117, 2017.

[137] N. Kotagiri, G. P. Sudlow, J. A. Walter, and S. Achilefu, "Breaking the depth dependency of phototherapy with Cerenkov radiation and low-radiance-responsive nanophotosensitizers," *Nat. Nanotechnol.*, vol. 10, no. 4, pp. 370–379, 2015.

[138] A. Kamkaew, L. Cheng, S. Goel, et al., "Cerenkov radiation induced photodynamic therapy using chlorin e6-loaded hollow mesoporous silica nanoparticles," *ACS Appl. Mater. Interfaces*, vol. 8, no. 40, pp. 26630–26637, 2016.

[139] N. Davies and B. C. Wilson, "Tetherless fiber-coupled optical sources for extended metronomic photodynamic therapy," *Photodiagnosis Photodyn. Ther.*, vol. 4, no. 3, pp. 184–189, 2007.

[140] S. Mordon, "New optical sources for interstitial and metronomic photodynamic therapy," *Photodiagnosis Photodyn. Ther.*, vol. 23, pp. 209–211, 2018.

[141] H. Homayoni, W. Chen, and IEEE. "Improving photodynamic therapy efficiency by synthesis of folic acid and protoporphyrin IX conjugated persistent luminescence nanoparticles as a new drug carrier," in *2014 40th Annual Northeast Bioengineering Conference (Annual IEEE Northeast Bioengineering Conference)*, 2014.

[142] W. Pan, G. L. Ning, J. H. Wang, and Y. Lin, "A novel synthesis of alkaline earth silicate phosphor $Sr_3MgSi_2O_8$: Eu^{2+},Dy^{3+}," *Chin. J. Chem.*, vol. 25, no. 5, pp. 605–608, 2007.

[143] H.-L. Tu, Y.-S. Lin, H.-Y. Lin, et al., "In vitro studies of functionalized mesoporous silica nanoparticles for photodynamic therapy," *Adv. Mater.*, vol. 21, no. 2, pp. 172–177, 2009.

[144] L. D. Hu, P. Y. Wang, M. Y. Zhao, et al., "Near-infrared rechargeable "optical battery" implant for irradiation-free photodynamic therapy," *Biomaterials*, vol. 163, pp. 154–162, 2018.

[145] L. Ma, X. J. Zou, B. Bui, W. Chen, K. H. Song, and T. Solberg, "X-ray excited ZnS:Cu,Co afterglow nanoparticles for photodynamic activation [Article]," *Appl. Phys. Lett.*, vol. 105, no. 1, p. 5, 2014.

[146] L. Song, P. P. Li, W. Yang, et al., "Low-dose X-ray activation of W(VI)-Doped persistent luminescence nanoparticles for deep-tissue photodynamic therapy [Article]," *Adv. Funct. Mater.*, vol. 28, no. 18, p. 10, 2018.

[147] W. P. Fan, N. Lu, C. Xu, et al., "Enhanced afterglow performance of persistent luminescence implants for efficient repeatable photodynamic therapy," *ACS Nano*, vol. 11, no. 6, pp. 5864–5872, 2017.

[148] S. K. Sun, J. C. Wu, H. Y. Wang, et al., "Turning solid into gel for high-efficient persistent luminescence-sensitized photodynamic therapy," *Biomaterials*, vol. 218, 2019.

[149] J. Wang, J. L. Li, J. N. Yu, H. W. Zhang, and B. B. Zhang, "Large hollow cavity luminous nanoparticles with near-infrared persistent luminescence and tunable sizes for tumor afterglow imaging and chemo-/photodynamic therapies," *ACS Nano*, vol. 12, no. 5, pp. 4246–4258, 2018.

[150] J. Yang, Y. Y. Zhao, Y. Q. Meng, et al., "Irradiation-free photodynamic therapy in vivo induced by enhanced deep red afterglow within NIR-I bio-window," *Chem. Eng. J.*, vol. 387, pp. 124067-1–124067-15, 2020.

[151] J. Wang, Y. J. Li, R. H. Mao, Y. Wang, X. P. Yan, and J. Liu, "Persistent luminescent nanoparticles as energy mediators for enhanced photodynamic therapy with fractionated irradiation," *J. Mater. Chem. B*, vol. 5, no. 29, pp. 5793–5805, 2017.

[152] H. M. Chen, X. L. Sun, G. D. Wang, et al., "LiGa5O8:Cr-based theranostic nanoparticles for imaging-guided X-ray induced photodynamic therapy of deep-seated tumors [Article]," *Mater. Horiz.*, vol. 4, no. 6, pp. 1092–1101, 2017.

[153] Z. L. Xue, X. L. Li, Y. B. Li, et al., "X-ray-Activated near-infrared persistent luminescent probe for deep-tissue and renewable in vivo bioimaging [Article]," *ACS Appl. Mater. Interfaces*, vol. 9, no. 27, pp. 22132–22142, 2017.

[154] Y. Liu, J.-M. Liu, D. Zhang, et al., "Persistent luminescence nanophosphor involved near-infrared optical bioimaging for investigation of foodborne probiotics biodistribution in vivo: a proof-of-concept study," *J. Agric. Food Chem.*, vol. 65, no. 37, pp. 8229–8240, 2017.

[155] Y. J. Li, C. X. Yang, and X. P. Yan, "Biomimetic persistent luminescent nanoplatform for autofluorescence-free metastasis tracking and chemophotodynamic therapy [Article]," *Anal. Chem.*, vol. 90, no. 6, pp. 4188–4195, 2018b.

[156] Y.-C. Lu, C.-X. Yang, and X.-P. Yan, "Radiopaque tantalum oxide coated persistent luminescent nanoparticles as multimodal probes for in vivo near-infrared luminescence and computed tomography bioimaging," *Nanoscale*, vol. 7, no. 42, pp. 17929–17937, 2015.

[157] A. Abdukayum, C.-X. Yang, Q. Zhao, J.-T. Chen, L.-X. Dong, and X.-P. Yan, "Gadolinium complexes functionalized persistent luminescent nanoparticles as a multimodal probe for near-infrared luminescence and magnetic resonance imaging in vivo," *Anal. Chem.*, vol. 86, no. 9, pp. 4096–4101, 2014.

[158] W. B. Dai, Y. F. Lei, S. Ye, E. H. Song, Z. Chen, and Q. Y. Zhang, "Mesoporous nanoparticles Gd_2O_3@mSiO(2)/ZnGa2O4: Cr^{3+},Bi^{3+} as multifunctional probes for bioimaging," *J. Mater. Chem. B*, vol. 4, no. 10, pp. 1842–1852, 2016.

[159] T. Maldiney, B.-T. Doan, D. Alloyeau, M. Bessodes, D. Scherman, and C. Richard, "Gadolinium-doped persistent nanophosphors as versatile tool for multimodal in vivo imaging," *Adv. Funct. Mater.*, vol. 25, no. 2, pp. 331–338, 2015.

[160] E. Teston, Y. Lalatonne, D. Elgrabli, et al., "Design, properties, and in vivo behavior of superparamagnetic persistent luminescence nanohybrids," *Small*, vol. 11, no. 22, pp. 2696–2704, 2015.

[161] R. Zou, S. M. Gong, J. P. Shi, et al., "Magnetic-NIR persistent luminescent dual-modal ZGOCS@MSNs@Gd2O3 core−shell nanoprobes for in vivo imaging [Article]," *Chem. Mater.*, vol. 29, no. 9, pp. 3938–3946, 2017.

[162] J. Yang, Y. Liu, Y. Zhao, et al., "Ratiometric afterglow nanothermometer for simultaneous in situ bioimaging and local tissue temperature sensing," *Chem. Mater.*, vol. 29, no. 19, pp. 8119–8131, 2017.

[163] T. Ai, W. Shang, H. Yan, et al., "Near infrared-emitting persistent luminescent nanoparticles for hepatocellular carcinoma imaging and luminescence-guided surgery," *Biomaterials*, vol. 167, pp. 216–225, 2018.

[164] B. B. Srivastava, A. Kuang, and Y. Mao, "Persistent luminescent sub-10 nm Cr doped $ZnGa_2O_4$ nanoparticles by a biphasic synthesis route," *Chem. Commun.*, vol. 51, no. 34, pp. 7372–7375, 2015.

[165] Z. Li, Y. Zhang, X. Wu, X. Wu, R. Maudgal, H. Zhang, et al., "In vivo repeatedly charging near-infrared-emitting mesoporous SiO_2/$ZnGa_2O_4$: Cr^{3+} persistent luminescence nanocomposites," *Adv. Sci.*, vol. 2, no. 3, p. 1500001, 2015.

[166] R. Zou, J. Huang, J. Shi, et al., "Silica shell-assisted synthetic route for mono-disperse persistent nanophosphors with enhanced in vivo recharged near-infrared persistent luminescence," *Nano Res.*, vol. 10, no. 6, pp. 2070–2082, 2017.

[167] A. Abdukayum, J.-T. Chen, Q. Zhao, and X.-P. Yan, "Functional near infrared-emitting Cr^{3+}/Pr^{3+} co-doped zinc gallogermanate persistent luminescent nanoparticles with superlong afterglow for in vivo targeted bioimaging," *J. Am. Chem. Soc.*, vol. 135, no. 38, pp. 14125–14133, 2013.

[168] Y. J. Li and X. P. Yan, "Synthesis of functionalized triple-doped zinc gallogermanate nanoparticles with superlong near-infrared persistent luminescence for long-term orally administrated bioimaging [Article]," *Nanoscale*, vol. 8, no. 32, pp. 14965–14970, 2016.

[169] A. Tuerdi and A. Abdukayum, "Dual-functional persistent luminescent nanoparticles with enhanced persistent luminescence and photocatalytic activity," *RSC Adv.*, vol. 9, no. 31, pp. 17653–17657, 2019.

[170] Q. Q. Wang, S. Y. Zhang, Z. W. Li, and Q. Zhu, "Near infrared-emitting Cr^{3+}/Eu^{3+} Co-doped zinc gallogermanate persistence luminescent nanoparticles for cell imaging [Article]," *Nanosc. Res. Lett.*, vol. 13, p. 9, 2018.

[171] D. Gourier, A. Bessiere, S. K. Sharma, et al., "Origin of the visible light induced persistent luminescence of Cr^{3+}-doped zinc gallate," *J. Phys. Chem. Solid*, vol. 75, no. 7, pp. 826–837, 2014.

[172] G. Y. Liu, S. C. Zhang, Y. H. Shi, et al., ""Wax-sealed" theranostic nanoplatform for enhanced afterglow imaging-guided photothermally triggered photodynamic therapy [Article]," *Adv. Funct. Mater.*, vol. 28, no. 42, p. 11, 2018.

[173] R. Abdurahman, C. X. Yang, and X. P. Yan, "Conjugation of a photosensitizer to near infrared light renewable persistent luminescence nanoparticles for photodynamic therapy [Article]," *Chem. Commun.*, vol. 52, no. 90, pp. 13303–13306, 2016.

[174] T. H. Shi, W. J. Sun, R. X. Qin, et al., "X-Ray-Induced persistent luminescence promotes ultrasensitive imaging and effective inhibition of orthotopic hepatic tumors," *Adv. Funct. Mater.*, vol. 30, pp. 2001166-1-2001166-9, 2020.

[175] G. Ramirez-Garcia, S. Gutierrez-Granados, M. A. Gallegos-Corona, et al., "Long-term toxicological effects of persistent luminescence nanoparticles after intravenous injection in mice [Article]," *Int. J. Pharm.*, vol. 532, no. 2, pp. 686–695, 2017.

[176] J. Botterman, J. J. Joos, and P. F. Smet, "Trapping and detrapping in $SrAl2O4$:Eu,Dy persistent phosphors: influence of excitation wavelength and temperature," *Phys. Rev. B*, vol. 90, no. 8, pp. 085147-1–085147-15, 2014.

[177] F. Clabau, X. Rocquefelte, T. Le Mercier, P. Deniard, S. Jobic, and M.-H. Whangbo, "Formulation of phosphorescence mechanisms in inorganic solids based on a new model of defect conglomeration," *Chem. Mater.*, vol. 18, no. 14, pp. 3212–3220, 2006.

[178] F. Clabau, X. Rocquefelte, S. Jobic, et al., "Mechanism of phosphorescence appropriate for the long-lasting phosphors Eu^{2+}-doped $SrAl_2O_4$ with codopants Dy^{3+} and B^{3+}," *Chem. Mater.*, vol. 17, no. 15, pp. 3904–3912, 2005.

[179] K. Van den Eeckhout, D. Poelman, and P. F. Smet, "Persistent luminescence in non-Eu^{2+}-doped compounds: a review," *Materials*, vol. 6, no. 7, pp. 2789–2818, 2013.

[180] K. Van den Eeckhout, P. F. Smet, and D. Poelman, "Persistent luminescence in Eu^{2+}-doped compounds: a review," *Materials*, vol. 3, no. 4, pp. 2536–2566, 2010.

[181] P. Dorenbos, "Mechanism of persistent luminescence in Eu^{2+} and Dy^{3+} codoped aluminate and silicate compounds," *J. Electrochem. Soc.*, vol. 152, no. 7, p. H107, 2005.

[182] A. Lecointre, B. Viana, Q. LeMasne, A. Bessiere, C. Chaneac, and D. Gourier, "Red long-lasting luminescence in clinoenstatite," *J. Lumin.*, vol. 129, no. 12, pp. 1527–1530, 2009.

[183] A. Bessiere, S. K. Sharma, N. Basavaraju, et al., "Storage of visible light for long-lasting phosphorescence in chromium-doped zinc gallate," *Chem. Mater.*, vol. 26, no. 3, pp. 1365–1373, 2014.

[184] Z. L. Xue, X. L. Li, Y. B. Li, et al., "A 980 nm laser-activated upconverted persistent probe for NIR-to-NIR rechargeable in vivo bioimaging [Article]," *Nanoscale*, vol. 9, no. 21, pp. 7276–7283, 2017b.

[185] F. Liu, Y. F. Chen, Y. J. Liang, and Z. W. Pan, "Phonon-assisted upconversion charging in $Zn_3Ga_2GeO_8$:Cr^{3+} near-infrared persistent phosphor [Article]," *Opt Lett.*, vol. 41, no. 5, pp. 954–957, 2016a.

[186] Y. Chen, F. Liu, Y. Liang, et al., "A new up-conversion charging concept for effectively charging persistent phosphors using low-energy visible-light laser diodes," *J. Mater. Chem. C*, vol. 6, no. 30, pp. 8003–8010, 2018.

[187] F. Liu, W. Yan, Y.-J. Chuang, Z. Zhen, J. Xie, and Z. Pan, "Photostimulated near-infrared persistent luminescence as a new optical read-out from Cr^{3+}-doped $LiGa_5O_8$," *Sci. Rep.*, vol. 3, no. 1, pp. 1–9, 2013.

[188] S. K. Sharma, D. Gourier, E. Teston, D. Scherman, C. Richard, and B. Viana, "Persistent luminescence induced by near infra-red photostimulation in chromium-doped zinc gallate for in vivo optical imaging," *Opt. Mater.*, vol. 63, pp. 51–58, 2017.

[189] G. Ramirez-Garcia, M. Martinez-Alfaro, F. d'Orlye, et al., "Photo-stimulation of persistent luminescence nanoparticles enhances cancer cells death [Article]," *Int. J. Pharm.*, vol. 532, no. 2, pp. 696–703, 2017b.

[190] H. Homayoni, L. Ma, J. Y. Zhang, et al., "Synthesis and conjugation of $Sr_2MgSi_2O_7$:Eu^{2+},Dy^{3+} water soluble afterglow nanoparticles for photodynamic activation," *Photodiagnosis Photodyn. Ther.*, vol. 16, pp. 90–99, 2016.

[191] J. Bradley, "A review of radiation dose escalation trials for non-small cell lung cancer within the radiation therapy oncology group," *Semin. Oncol.*, vol. 32, pp. 111–113, 2005.

[192] D. A. Palma, W. F. A. R. Verbakel, K. Otto, and S. Suresh, "New developments in arc radiation therapy: a review," *Canc. Treat. Rev.*, vol. 36, no. 5, pp. 393–399, 2010.

[193] J. Kim, H. S. Kim, N. Lee, T. Kim, H. Kim, T. Yu, et al., "Multifunctional uniform nanoparticles composed of a magnetite nanocrystal core and a mesoporous silica shell for magnetic resonance and fluorescence imaging and for drug delivery," *Angew. Chem.*, vol. 120, no. 44, pp. 8566–8569, 2008.

[194] B.-M. Liu, W.-J. Gan, S.-Q. Lou, et al., "X-ray-activated, UVA persistent luminescent materials based on Bi-doped $SrLaAlO_4$ for deep-Seated photodynamic activation," *J. Appl. Phys.*, vol. 129, no. 12, p. 120901, 2021.

[195] X. Sun, J. P. Shi, X. Y. Fu, Y. Yang, and H. W. Zhang, "Long-term in vivo biodistribution and toxicity study of functionalized near-infrared persistent luminescence nanoparticles," *Sci. Rep.*, vol. 8, pp. 10595-1–10595-11, 2018.

[196] Y. Jiang, Y. Li, C. Richard, D. Scherman, and Y. S. Liu, "Hemocompatibility investigation and improvement of near-infrared persistent luminescent nanoparticle $ZnGa_2O_4:Cr^{3+}$ by surface PEGylation," *J. Mater. Chem. B*, vol. 7, no. 24, pp. 3796–3803, 2019.

[197] T. Lécuyer, M.-A. Durand, J. Volatron, et al., "Degradation of $ZnGa_2O_4:Cr^{3+}$ luminescent nanoparticles in lysosomal-like medium," *Nanoscale*, vol. 12, no. 3, pp. 1967–1974, 2020.

[198] D. Van der Heggen, J. J. Joos, D. C. Rodríguez Burbano, J. A. Capobianco, and P. F. Smet, "Counting the photons: determining the absolute storage capacity of persistent phosphors," *Materials*, vol. 10, no. 8, p. 867, 2017.